Author Manuscript

Author Manuscript

Author Manuscript

Author Manuscript

HHS Public Access

Author manuscript

Nature. Author manuscript; available in PMC 2019 December 01.

Published in final edited form as:

Nature. 2018 December ; 564(7734): 119–124. doi:10.1038/s41586-018-0709-7.

VCAM-1+ macrophages guide the homing of HSPCs to a vascular niche

Dantong Li[1,2,10], **Wenzhi Xue**[1,10], **Mei Li**[1,2,10], **Mei Dong**[1], **Jianwei Wang**[1], **Xianda Wang**[1], **Xiyue Li**[1], **Kai Chen**[1], **Wenjuan Zhang**[1], **Shuang Wu**[1], **Yingqi Zhang**[3], **Lei Gao**[1,4], **Yujie Chen**[5], **Jianfeng Chen**[6], **Bo O. Zhou**[6], **Yi Zhou**[7], **Xuebiao Yao**[8], **Lin Li**[6], **Dianqing Wu**[9], and **Weijun Pan**[1,2,*]

[1]Key Laboratory of Tissue Microenvironment and Tumor, CAS Center for Excellence in Molecular Cell Science, Shanghai Institute of Nutrition and Health, Shanghai Institutes for Biological Sciences, University of Chinese Academy of Sciences, Chinese Academy of Sciences (CAS), Shanghai, China.

[2]Key Laboratory of Stem Cell Biology, Shanghai Jiao Tong University School of Medicine (SJTUSM) & Shanghai Institutes for Biological Sciences (SIBS), CAS, Shanghai, China.

[3]Department of Orthopedic Surgery, Tongji Hospital, Tongji University School of Medicine, Shanghai, China.

[4]Key Laboratory of Genome Sciences and Information, Beijing Institute of Genomics, CAS, Beijing, China.

[5]Key Laboratory of Computational Biology, CAS-MPG Partner Institute for Computational Biology, Shanghai Institute of Nutrition and Health, Shanghai Institutes for Biological Sciences, University of Chinese Academy of Sciences, CAS, Shanghai, China.

[6]State Key Laboratory of Molecular Biology, CAS Center for Excellence in Molecular Cell Science, Institute of Biochemistry and Cell Biology, Shanghai Institutes for Biological Sciences, CAS, Shanghai, China.

[7]Stem Cell Program and Division of Hematology/Oncology, Boston Children's Hospital and Dana-Farber Cancer Institute, Harvard Medical School, Boston, MA, USA.

Reprints and permissions information is available at http://www.nature.com/reprints.

[*]**Correspondence and requests for materials** should be addressed to W.P. weijunpan@sibs.ac.cn.

Author contributions D.L., W.X. and W.P developed the concepts and designed the experiments. D.L., W.X. and M.L. performed the experiments and analysed data. M.D. performed ENU screening and positional cloning. J.W. assisted with 3D reconstruction and HSPC retention heat-map analysis. X.W. and X.L. assisted the experiments and data analysis during revision. K.C., W.Z. and S.W. assisted with the schematic illustration of the working model for HSPC homing. YJ.C. assisted with imaging with Zeiss 880 and Y Zhang assisted with 3D-reconstruction analysis. J.C. and X.Y supported experiments and provided ideas about the distinct role of VCAM-1 in different cell populations. L.G., B.O.Z., Y Zhou, L.L. and D.W. provided ideas and discussions throughout the project. J.C., B.O.Z., Y Zhou, X.Y and L.L. revised the manuscript. D.L., D.W. and W.P wrote the paper. W.P supervised the project.

Competing interests The authors declare no competing interests.

Online content

Any methods, additional references, Nature Research reporting summaries, source data, statements of data availability and associated accession codes are available at https://doi.org/10.1038/s41586–018-0709–7.

Additional information

Extended data is available for this paper at https://doi.org/10.1038/s41586-018-0709-7.

Supplementary information is available for this paper at https://doi.org/10.1038/s41586-018-0709-7.

Publisher's note: Springer Nature remains neutral with regard to jurisdictional claims in published maps and institutional affiliations.

Author Manuscript Author Manuscript Author Manuscript Author Manuscript

[8]CAS Center for Excellence in Molecular Cell Science, University of Science and Technology of China, Hefei, China.

[9]Department of Pharmacology, Vascular Biology and Therapeutic Program, School of Medicine, Yale University, New Haven, CT, USA.

[10]These authors contributed equally: Dantong Li, Wenzhi Xue, Mei Li.

Abstract

Haematopoietic stem and progenitor cells (HSPCs) give rise to all blood lineages that support the entire lifespan of vertebrates[1]. After HSPCs emerge from endothelial cells within the developing dorsal aorta, homing allows the nascent cells to anchor in their niches for further expansion and differentiation[2–5]. Unique niche microenvironments, composed of various blood vessels as units of microcirculation and other niche components such as stromal cells, regulate this process[6–9]. However, the detailed architecture of the microenvironment and the mechanism for the regulation of HSPC homing remain unclear. Here, using advanced live imaging and a cell-labelling system, we perform high-resolution analyses of the HSPC homing in caudal haematopoietic tissue of zebrafish (equivalent to the fetal liver in mammals), and reveal the role of the vascular architecture in the regulation of HSPC retention. We identify a VCAM-1$^+$ macrophage-like niche cell population that patrols the inner surface of the venous plexus, interacts with HSPCs in an ITGA4-dependent manner, and directs HSPC retention. These cells, named ‘usher cells’, together with caudal venous capillaries and plexus, define retention hotspots within the homing microenvironment. Thus, the study provides insights into the mechanism of HSPC homing and reveals the essential role of a VCAM-1$^+$ macrophage population with patrolling behaviour in HSPC retention.

In vertebrates, the establishment of the HSPC pool is a dynamic process that requires not only the HSPC fate specification from the haemogenic endothelium, but also their subsequent homing to distinct anatomic sites[2–5]. In the zebrafish, HSPCs are initially formed in the ventral wall of the dorsal aorta in the aorta-gonad-mesonephros (AGM) region[3,4]. The nascent HSPCs then migrate to the caudal haematopoietic tissue (CHT) and kidney marrow, which are the haematopoietic tissues equivalent to mammalian fetal liver and bone marrow, respectively, where the HSPCs undergo rapid expansion and differentiation to support larval and adult haematopoiesis[2,10]. However, how HSPCs migrate to and finally colonize these tissues remains poorly understood.

To investigate these unknown mechanisms, we carried out a large-scale forward genetics screen in zebrafish for mutants that display HSPC homing defects. The mutant line cas005 showed severe defects in definitive haematopoiesis, but normal primitive haematopoiesis and vascular morphogenesis (Extended Data Fig. 1a, b, e, g). Although the haemogenic endothelium in *mut*^{cas005} was intact, as revealed by whole-mount in situ hybridization (WISH) results of the nascent HSPC marker *runx1*[11] (a key transcription factor that regulates nascent HSPC emergence), the number of HSPCs in the mutant CHT was severely reduced (Extended Data Fig. 1c–e, g), without increased HSPC apoptosis (Extended Data Fig. 1f) compared to the wild-type CHT.

Author Manuscript Author Manuscript Author Manuscript Author Manuscript

The genetic mutation was mapped to a loss-of-function mutation in the *integrin alpha 4 (itga4)* gene by positional cloning (Extended Data Fig. 2a–c). Indeed, morpholino-mediated knockdown of *itga4* expression (Extended Data Fig. 2e–g) or a second zebrafish *itga4*^{cas010} mutant generated by CRISPR-Cas9[12] (Extended Data Fig. 2b–d) displayed similar phenotypes to that of *mut*^{cas005}, which was hence renamed as *itga4*^{cas005}.

WISH analysis showed that *itga4* expression was enriched in both the AGM and the CHT in a *runx1*11- and *myb*[13] (another key transcription factor that regulates nascent HSPC migration into circulation-dependent manner (Extended Data Fig. 2h). Conversely, *runx1* enhancer[14]-directed definitive HSPC re-expression of wild-type *itga4* could rescue the *itga4* mutant defects (Extended Data Fig. 2i–k), indicating an HSPC cell-autonomous role of ITGA4.

The defective definitive haematopoiesis in zebrafish *itga4* mutants is consistent with a previous report[15]. The VLA-4 integrin, composed of α_4 *(itga4)* and β_1 *(itgb1)* subunit, is predominantly expressed on HSPCs in mammals in early embryogenesis[16]. In mice, the a_4 integrin is essential for normal haematopoietic development in the fetal liver[15,17], and inhibition of α_4 could mobilize HSPCs from fetal livers by interfering with the homing and retention process[18,19]. However, the precise mechanism by which IT GA4 regulates HSPC homing remains largely unknown.

To achieve real-time characterization of HSPC homing to, and retention in, the CHT, we took advantage of the transgenic line *Tg(kdrl:Dendra2),* in which the *kdrl* gene promoter drives the expression of the photoconvertible Dendra2 fluorescent protein in the entire vasculature. At 36 hours post-fertilization (h.p.f.), we converted the green fluorescence of Dendra2$^+$ endothelial cells in the AGM to red (Extended Data Fig. 3a). Consistent with previous reports[3,4], a substantial number of endothelial cells converted by endothelial-to-haematopoietic transition emerged from the aortic ventral wall into the sub-aortic space, subsequently entered the blood circulation, and finally colonized the CHT by 48–50 h.p.f. (Extended Data Fig. 3a, b).

These photoconverted red Dendra2$^+$ cells in the CHT were found to carry *runx1* transcripts (Extended Data Fig. 3b). In addition, the knockdown of *runx1* or *myb* expression[13] significantly reduced the number of photoconverted red Dendra2$^+$ cells in the CHT (Extended Data Fig. 3c, d). These results confirmed that the photoconverted red Dendra2$^+$ cells homing to the CHT were nascent HSPCs.

Thus, we were able to characterize the entire process and individual HSPC homing–retention events in the CHT. We found that the lodgement of HSPCs initially took place at approximately 48–50 h.p.f., and the number of lodged HSPCs markedly increased over 24 h. However, in the itga4-mutant embryos, HSPC retention was barely detectable (Fig. 1a, c and Supplementary Video 1). More specifically, the average retention time of HSPCs in wild-type embryos is close to 30 min, whereas the HSPCs in the *itga4* mutants went through the CHT quickly with very short retention times (average retention time of 4 min) (Fig. 1d, e, Extended Data Fig. 3e and Supplementary Video 2). The functional consequence of the disrupted HSPC retention was markedly reduced downstream haematopoietic lineages

Author Manuscript Author Manuscript Author Manuscript Author Manuscript

(Extended Data Figs. 1e, g, 2f, g). We thus defined a successful HSPC retention event in the CHT as the lodgement of HSPCs for a period of more than 30 min (over 20% of HSPCs in the wild-type embryos, but less than 2% of HSPCs in the *itga4* mutants).

It has been proposed that HSPCs reside in the anatomically defined niche, where they receive and integrate regulatory signals from the niche cells and extracellular matrices[6,7,20] for their expansion and differentiation. To understand the tendency of HSPC retention, we traced individual HSPCs and correlated their retention time with the dorsal-ventral relative location. This scatterplot analysis revealed that the longer HSPCs resided in the CHT, the greater was their tendency to reach the dorsal part of the caudal venous plexus (CVP) (Extended Data Fig. 4a). Next, we analysed the frequency of HSPCs' appearance in the entire CHT over an 8-h time period. Unexpectedly, the retention of HSPCs was not evenly distributed in the dorsal part of the CVP, and instead the cells frequently occurred in several regions of the CHT in wild-type embryos. We referred to these regions as the retention 'hotspots' (Fig. 1f and Extended Data Fig. 4b, c).

These retention hotspots are largely localized at the venous capillary confluence points that are connected to the CVP, in which the velocity of circulating photoconverted HSPCs is notably reduced (Extended Data Fig. 5a). HSPCs that entered the CHT either from the intersegmental vessel (ISV) or from the CVP (Extended Data Fig. 5b–e and Supplementary Video 3) were sharply decelerated. We also found that most HSPCs that remained for more than 30 min were in the venous capillaries, which have similar diameters to that of HSPCs (Fig. 1b, Extended Data Fig. 6a–f, h, Supplementary Video 4). In the *itga4* mutants, the retention hotspots were not evident (Extended Data Fig. 4d). However, there was no significant difference in the number, size or confluence points of the vascular architecture between wildtype embryos and *itga4* mutants (Extended Data Fig. 6g, h). These observations led us to hypothesize that other niche components might be needed for HSPCs to enter the venous capillaries in an ITGA4-dependent manner.

Vascular cell adhesion molecule-1 (VCAM-1) is known as the major ligand for VLA-4 in mammalian cells[21,22]. According to the ZFIN database (http://zfin.org/ZDB-GENE-070209–238), zebrafish *vcam1* (also known as *vcam1b)* was specifically expressed in the cranial region, heart and the CHT at around 30 h.p.f. To evaluate the function of VCAM-1 in definitive haematopoiesis, we generated a *vcam1*^{cas011} mutant (Extended Data Fig. 7a, b). The mutants resembled the defects in homing and definitive haematopoiesis observed in the *itga4* mutants (Fig. 2a, Extended Data Figs. 2f, g, 7c–f, Supplementary Video 5), indicating that the ITGA4-VCAM-1 axis has an evolutionarily conserved role in nascent HSPC homing and retention[16,23].

Immunofluorescence staining showed that endogenous VCAM-1 was strongly expressed on cells that are mostly distributed at the dorsal CVP, where HSPCs show preferential lodgement (Fig. 2b). In addition, VCAM-1 protein was also weakly expressed on some of the venous endothelial cells in the CHT (Extended Data Fig. 7g). Importantly, the VCAM-1^{+} non-endothelial cells in the CHT were always next to HSPCs (Fig. 2c, Extended Data Fig. 7h), which were neither previously described *cxcl12a:DsRed*$^{+}$ cells nor somite-derived stromal reticular cells[8,9](Extended Data Fig. 7i, j). By contrast, we found that almost all the

Author Manuscript Author Manuscript Author Manuscript Author Manuscript

VCAM-1$^+$ non-endothelial cells were GFP$^+$ in the macrophage-specific *Tg(mpeg1:eGFP)* transgenic line in the CHT (Fig. 2d). Meanwhile, about 45% of *mpeg1*$^+$ cells in the CHT are VCAM-1$^+$, and there are on average 13 VCAM-1$^+$ macrophage-like cells per CHT (Extended Data Fig. 8d) that express the macrophage markers *mfap4, csflra* and *spila* with high overlapping rates (Extended Data Fig. 8a and Supplementary Table 2). Thus, these VCAM-1$^+$ non-endothelial cells in the CHT are likely to be a subtype of macrophages.

To characterize the potential function of these VCAM-1$^+$ macrophage-like cells in the homing and retention of HSPCs, we either depleted macrophages using metronidazole (MTZ) (loss-of-function analysis; Extended Data Fig. 8b–f), or transiently expressed wild-type *vcaml* in *mpegl*-positive macrophage cells in *vcaml* mutants (gain-of-function analysis; Extended Data Fig. 8b–g). MTZ depletion of macrophages did not affect HSPC emergence (Extended Data Fig. 8c), but caused impaired HSPC lodgement (Fig. 2e, f, Extended Data Fig. 8f) and defective definitive haematopoiesis (Extended Data Fig. 8e), indicating that macrophages are essential for HSPC retention. However, when the behaviour of HSPCs was compared with those of the *vcam-1*^{cas011} mutants, we found that although HSPCs in macrophage-depleted embryos did not successfully lodge in the CHT, they could flow slowly in the vasculature, suggesting that endothelial VCAM-1 might have a role in the initiation of HSPC rolling on the dorsal endothelium bed (Fig. 2e, Extended Data Figs. 4e, 8f and Supplementary Video 6), consistent with previous reports[24].

The re-expression of *vcaml* exclusively in *mpegl*-positive cells could significantly restore HSPC retention (Fig. 2g, Extended Data Figs. 4e, 8e–g and Supplementary Video 6). The incomplete rescue of the retention phenotype suggests that the interaction of HSPCs with the CVP endothelium might also have a role by slowing down HSPCs to increase the chance for HSPC retention, even though the HSPC-CVP endothelium interaction is not absolutely required for HSPC retention.

To determine when the VCAM-1$^+$ macrophages appear in the CHT, we performed a time-course analysis of VCAM-1 expression from 28 to 48 h.p.f. The immunofluorescence results demonstrated that the VCAM-1$^+$ macrophages first appeared in the CHT at 32 h.p.f. (Fig. 3a). The VCAM-1$^+$ macrophages in the CHT were absent in the *vcam1*^{cas011} mutants and independent of HSPC deficiency in either *itga4*^{cas005} or *runx1*^{w84x} mutants at 54 h.p.f. (Fig. 3b). Because the VCAM-1$^+$ macrophages are present in the niche before the appearance of aorta-derived definitive HSPCs, these macrophages probably arise from the primitive macrophage lineage at this time point. We labelled the primitive macrophages by applying photoconversion on the *Tg(mpeg1:Gal4,UAS:Kaede)* line, and found that some macrophages from the rostral blood island[25] at 18 h.p.f. migrated to the CHT, and were VCAM-1$^+$ (Extended Data Fig. 8h).

To characterize the behaviour and function of the VCAM-1$^+$ macrophages in live animals further, we labelled VCAM-1$^+$ macrophages with an anti-VCAM-1^{647} antibody. The live imaging showed a nearly identical cell distribution pattern to that revealed by anti-VCAM-1 immunofluorescence (Extended Data Fig. 9a). Live staining with the antibody remained stable for at least 8 h after intravascular antibody injection, without affecting definitive

Author Manuscript Author Manuscript Author Manuscript Author Manuscript

haematopoiesis, as demonstrated by quantitative *myb* WISH analysis (Extended Data Fig. 9b–d).

Notably, these VCAM-1$^+$ macrophages slowly patrolled on the inner sides, especially the dorsal CVP (Fig. 3c, Extended Data Fig. 9e, Supplementary Video 7). HSPCs, entering from either the ISV or the CVP into the CHT, always pass by the capillary confluence point, which leads to frequent interactions of HSPCs with the VCAM-1$^+$ macrophages.

After quantitative analysis of more than 100 VCAM-1$^+$ macrophage–HSPC interactions and subsequent events (Fig. 4a, Supplementary Table 3), we found that, on average, each interaction lasted approximately 30 min. About 60% of the HSPCs left the CHT through the venous plexus without retention (6–30 min), whereas around 40% of HSPCs could remain in the CHT for more than 30 min.

Among these lodged HSPCs, about 75% interacted with VCAM-1$^+$ macrophages at the entrance of dorsal venous capillaries. With the guidance of VCAM-1$^+$ macrophages, 20% could finally enter the venous capillaries and remained for more than 120 min. We defined this as ‘type I’ retention (Fig. 4a, Extended Data Fig. 9f, Supplementary Video 8). Conversely, 25% of the lodged HSPCs interacted with VCAM-1$^+$ macrophages within the CVP, and then 6.25% were surrounded by an ‘endothelial pocket’[14] structure, leading to the ‘type II’ retention (Fig. 4a, b, Extended Data Fig. 9f, Supplementary Video 9). HSPCs that successfully interacted with VCAM-1$^+$ macrophages (for more than 30 min) but failed to be guided into the vascular niche (55% as pre-type I and 18.75% as pre-type II retention) were termed ‘type 0’ retention. Notably, HSPCs have an increased chance of interacting with VCAM-1$^+$ macrophages at venous capillary confluence points connected to the CVP where dorsal venous capillaries are also distributed and the hotspots of HSPCs retention were observed (Fig. 1f).

In *itga4*^{cas010} mutants, HSPCs encountered but did not interact with VCAM-1$^+$ macrophages. They could not roll inside the vasculature, enter venous capillaries or be enveloped by endothelium. Instead, the HSPCs went quickly through the CHT (Extended Data Fig. 9g and Supplementary Video 10). Thus, the interaction mediated by ITGA4 and VCAM-1 has an essential role in HSPC homing and retention in the niche. Together with the feature that VCAM-1$^+$ macrophages patrol at the dorsal CVP, we named these VCAM-1$^+$ macrophages ‘usher’ cells. In addition, HSPCs retention in *vcam1*^{cas011} mutants with macrophage-specific *vcam1* re-expression restored the occurrence of type II retention, indicating that the loss of vascular VCAM-1 is not sufficient to disrupt the vascular ‘cuddling’ structure (Extended Data Fig. 9h).

In this study, we mainly focused on the period of 48–60 h.p.f. at the initiation of HSPC homing because current imaging technology and transgenic lines do not allow the symmetry division to be distinguished from the asymmetry one, although most of the HSPC division in the CHT occurred in the vascular niche (66% in type I, 30% in type II retention). Morphology-based asymmetry division of HSPCs was previously reported in the vascular cuddling structure[14]; however, lineage-specific reporter lines with rapid responses are

Author Manuscript Author Manuscript Author Manuscript Author Manuscript

required in future studies to understand how the dynamic HSPC-niche interaction is coordinated with HSPC division.

We show that the behaviour of usher cells correlates with the retention of HSPCs in the CHT. It has been reported that macrophages promote the retention of HSPCs[26,27]. However, it is still not clear how the usher cells as well as niche cells express other molecules that recognize receptors on the HSPCs, serving as additional permissive signals for the entry of HSPCs into the niches. In addition, the *itga4* mutant specifically impaired definitive haematopoiesis in the CHT, but not that in the thymus or kidney marrow, indicating different homing mechanisms might govern the lodgement of HSPCs into different niches (Extended Data Fig. 1e, g). Future studies are warranted to investigate these important questions.

METHODS

Zebrafish husbandry

The zebrafish facility and study were approved by the Animal Research Advisory Committee of Institute of Nutrition and Health, SIBS, CAS, and zebrafish were maintained according to the guidelines of the Institutional Animal Care and Use Committee. The Tubingen and WIK wild-type strains were used in this study. The *runx1*^{w84x} mutant line[28] and transgenic lines *Tg(gata1:DsRed)29, Tg(mpx:eGFP)30, Tg(lyz:DsRed)31, Tg(kdrl:Dendra2)32, Tg(kdrl:eGFP)33, Tg(mpeg1*:*Gal4, UAS:NfsB-mCherry)*[34], *Tg(UAS:Kaede)35, Tg(cxcl12a*:*DsRed)*[8], Tg(*tcf.eGFP)*9‘36 and Tg(*mpeg1*:eGFP)[37] were described previously.

Genetic mapping and mutation identification of zebrafish *cas005* mutant

The *mut*^{005} line was identified in a large-scale N-ethyl-N-nitrosourea (ENU) -mutagenized F2 family screen based on the *myb* expression phenotype of 5 days post-fertilization (d.p.f.) zebrafish embryos. The ENU screen and positional cloning were performed as described previously[38]. The mutation was mapped to chromosome 9 by bulk segregation analysis with sequence length polymorphism (SSLP) markers[39]. Fine mapping was carried out to narrow down the genetic interval, and the mutation was finally flanked by two SSLP markers, z8363 and zK165L22. The cDNAs of candidate genes in the range were cloned and sequenced from siblings and mutants, and the putative mutation was confirmed by sequencing genomic DNA of individual mutant embryos. All primers used for this study are provided in Supplementary Table 1.

Plasmid construction

The zebrafish *vcam1* (also known as *vcam1b,* accession number: ZDB-GENE-070209–238) was cloned and inserted into the Tol2 backbone between the *UAS* promoter and polyA. The *runx1* +23 enhancer followed by P2A and in-frame mCherry was cloned into the Tol2 backbone, and the zebrafish *itga4* (accession number: ZDB-GENE-110411–108) was amplified and inserted between the *runx1* enhancer and P2A.The sequences of *vcam1* and *itga4* were verified by sequencing. The *runx1* +23 enhancer[14] and *UAS* promoter[40] were cloned as previously reported.

Author Manuscript Author Manuscript Author Manuscript Author Manuscript

Microinjection and CRISPR–Cas9 mutagenesis

Morpholino oligonucleotides were designed and purchased from Gene Tools. The morpholino oligonucleotides used in this study give the same phenotypes as mutants. The *itga4, runx1*[41], myb[13] and *vcam1* morpholino oligonucleotides were injected into one-cell-stage embryos as previously described[42]. Transient transgenic constructs within Tol2 vectors (40 pg) were microinjected into one-cell-stage embryos with Tol2 transposase mRNA (40 pg)[43]. For CRISPR-Cas9-mediated generation of zebrafish mutants *(itga4*^{cas010} and *vcam1*^{cas011}*),* guide RNAs (RNAs) were designed to target genes according to methods previously described[44]. The zebrafish codon-optimized *Cas9* mRNA was synthesized from the pCS2-nCas9n plasmid (Addgene, plasmid47929)[12] and gRNAs were in vitro synthesized using the MAXIscript T7 kit (Ambion). The gRNAs (100 pg) were microinjected into one-cell-stage embryos with *Cas9* mRNA (300 pg).

Conventional WISH, FISH and RNA scope in situ analysis

The *myb*45, *scl*[46], *gata146, pu.146, kdrl45, runx147, hbae1.145,* mpx[45], lyz[45], *itga4, mfap4*[48] and *csf1ra*[48] probes were transcribed in vitro by T3 or T7 polymerase (Ambion) with Digoxigenin RNA Labelling Mix (Roche). Conventional and fluorescence whole-mount in situ hybridization (WISH and FISH) was described previously[49]. The penetrance of the indicated phenotype is shown in the bottom right of each panel (Extended Data Figs. 1a–e, g, 2d, e, h, 7d–f and 9d) and the embryos were genotyped after WISH and before phenotypic analysis (Extended Data Figs. 2d, j, k, 7d–f, 8e and 9b). Images of conventional WISH were mounted in 4% methylcellulose and captured by Olympus SZX16 microscope with Olympus DP80 CCD. In FISH and immunofluorescence double-staining, embryos were stained with cy3 or cy5 (TSA system, Perkin Elmer), followed by immunofluorescence, and then imaged by Zeiss LSM880 confocal microscope. RNA scope was conducted with probe *runx1* (P/N: 433351, ACDBio) and negative control probe (REF: 320871, ACDBio). RNA scope procedure was performed as previously described[50], and imaged by Olympus FV1000 Fluoview scanning confocal microscope. A list of oligonucleotides used to amplify these probes is provided in Supplementary Table 1.

Immunofluorescence staining and usher cell live immunolabelling

Immunofluorescence staining was performed as previously described[51], with mouse anti-DsRed (Abcam), mouse anti-eGFP (Abmart), rabbit anti-VCAM-1 antibody (immunized by 180–300 amino acids of zebrafish VCAM-1 protein, Abclonal), AF488/546/647-conjugated secondary antibody (Life Technologies) and TUNEL assay kit (Roche). Images were collected using Olympus FV1000 Fluoview scanning confocal, Zeiss LSM710 confocal and Zeiss LSM880 confocal microscope and the embryos were genotyped following imaging analysis (Fig. 3b and Extended Data Fig. 8d). For live labelling of usher cells, VCAM-1 antibody (Abclonal) was conjugated with Alexa Fluor 647 dye and purified by Microscale Protein Labelling Kit (Invitrogen, A30009). Each embryo was injected 1 nl (0.4 ng) at the common cardinal vein into the circulation at 50 h.p.f. In vivo monitoring started from 2 h after injection and this live labelling is stable for more than 8 h[52]. Time-lapse intravital imaging was acquired by Zeiss LSM880 confocal microscope.

Author Manuscript Author Manuscript Author Manuscript Author Manuscript

Inducible macrophage-specific cell depletion

As previously reported, MTZ-mediated cell depletion was performed on *Tg(mpeg1:GAL4,UAS:NfsB-mCherry, kdrl:Dendra2)*[34,53] transgenic zebrafish embryos. Embryos from 24 to 60 h.p.f. were treated with freshly prepared 10 mM MTZ (Sigma) in 0.2% DMSO (dimethylsulfoxide) solution protected from light until the evaluation finished, then rinsed with embryo water three times.

Confocal microscope photoconversion and time-lapse live imaging analysis

The photoconversion of irreversible monomeric green-to-red fluorescent protein Dendra2[54,55] expressed following specific promoter was conducted with a 405-nm laser for 30 s by an Olympus FV1000 Fluoview scanning confocal microscope. For the HSPC labelling system, the ventral endothelium of dorsal aorta (between somites 8 and 17) of *Tg(kdrl:Dendra2)* embryos was exposed to a beam of405 nm ultraviolet (UV) laser light under a confocal microscope at 30–36 h.p.f. without affecting the normal endothelial-to-haematopoietic transition process, compared with that in untreated embryos[4]. The efficiency of cell labelling was confirmed under fluorescent microscope 8 h after photoconversion. The zebrafish with precise and bright photoconverted Dendra2 (red) cells were selected for further analysis. For the macrophage labelling system, the rostral blood island of *Tg(mpeg1:Gal4,UAS:Kaede)* zebrafish embryos was photoconverted at 18 h.p.f., followed by anti-VCAM-1[647] injection at 50 h.p.f., and imaging at 52 h.p.f. using Zeiss LSM880 confocal microscope.

For time-lapse imaging, embryos were anaesthetized with 0.03% Tricaine (Sigma), and mounted in 1.5% low melting point agarose in a 60-mm dish. The embryos were scanned at 28.5 °C under an Olympus FV1000 Fluoview scanning confocal microscope with 20× water immersion objective, *z*-stalks were acquired with a step size of 3 μm within an interval of 3 min over several hours. To observe more details between HSPCs and vascular niche, images were collected using a Zeiss LSM880 confocal by 40 × water immersion objective; *z*-stalks were acquired with a size of 3 pm for over 8 h. The Zeiss LSM880 confocal allowed imaging of several embryos within a 2–5-min interval using a moving XY stage, as well as acquisition of *z*-stacks through the tissue in multiple channels. Note that 10 h is the maximum experimental duration of live-imaging analysis without phototoxicity. The embryos were genotyped following live-imaging analysis (Fig. 1a, c–e, 2a, e–g and Extended Data Figs. 3e, 4d, e, 6g, h, 7c, 8f, g, 9a, e, g, h).

Imaging data processing and rendering was performed in FV10-ASW 3.0 Viewer (Olympus), ZEN 2.1 (ZEISS), Imaris (Bitplane) and ImageJ (NIH). The retention time and location information that each HSPC appears in the CHT was exported by Imaris ‘Spots’ module and programmed by Python into retention heatmap (https://pypi.python.org/pypi/pyheatmap). The velocity of photoconverted HSPCs in the CHT was measured with the axial line scanning (ALS) as previously described[56–58]. Zeiss LSM880 equipped with Airyscan function was applied to capture high-resolution fluorescent images, followed with 3D reconstruction by Materialise software (including Mimics Medical and 3-matic Medical).

Author Manuscript Author Manuscript Author Manuscript Author Manuscript

Statistical analysis

All statistical analysis was performed using Graphpad Prism 7 software using the two-tailed Student's t-test. Centre values denote the mean, and error values denote s.e.m. (Fig. 1c and Extended Data Figs. 1f, 2f, 3d, 6h, 8c, d, 9f). The biologically independent sample size (n) was shown in the relevant figure panel (Fig. 1c and Extended Data Figs. 1f, 2f, j, 3d, 6h, 8c–e, 9b, f, h). All experiments in this study were repeated independently at least three times. For representative images, we have performed imaging on 5–10 embryos per independent experiments and repeated at least three times independently to find the most representative images (Figs. 1a, 2b–e, 3a–c, 4 and Extended Data Figs. 2k, 3e, 5a, c, d, 6e–g, 7c, g–j, 8a, c, g, h, 9a, c, e, g). The graphs in Fig. 1d and Extended Data Fig. 8f show individual values in three embryos per group separately. In Fig. 1f and Extended Data Fig. 4b–e, imaging was performed on one embryo per independent experiment, repeated three times independently, and three images were chosen for the analysis. ****$P < 0.0001$. No statistical methods were used to predetermine sample size. The experiments were not randomized, and investigators were not blinded to allocation during experiments and outcome assessment.

Reporting summary

Further information on research design is available in the Nature Research Reporting Summary linked to this paper.

Data availability

Any Methods, including any statements of data availability and Nature Research reporting summaries, along with any additional references and Source Data files, are available in the online version of the paper. 3D reconstruction of vessel surrounding HSPCs in retention hotspot is deposited at http://www.biosino.org/node/project/detail/OEP000169.

Extended Data

Author Manuscript Author Manuscript Author Manuscript Author Manuscript

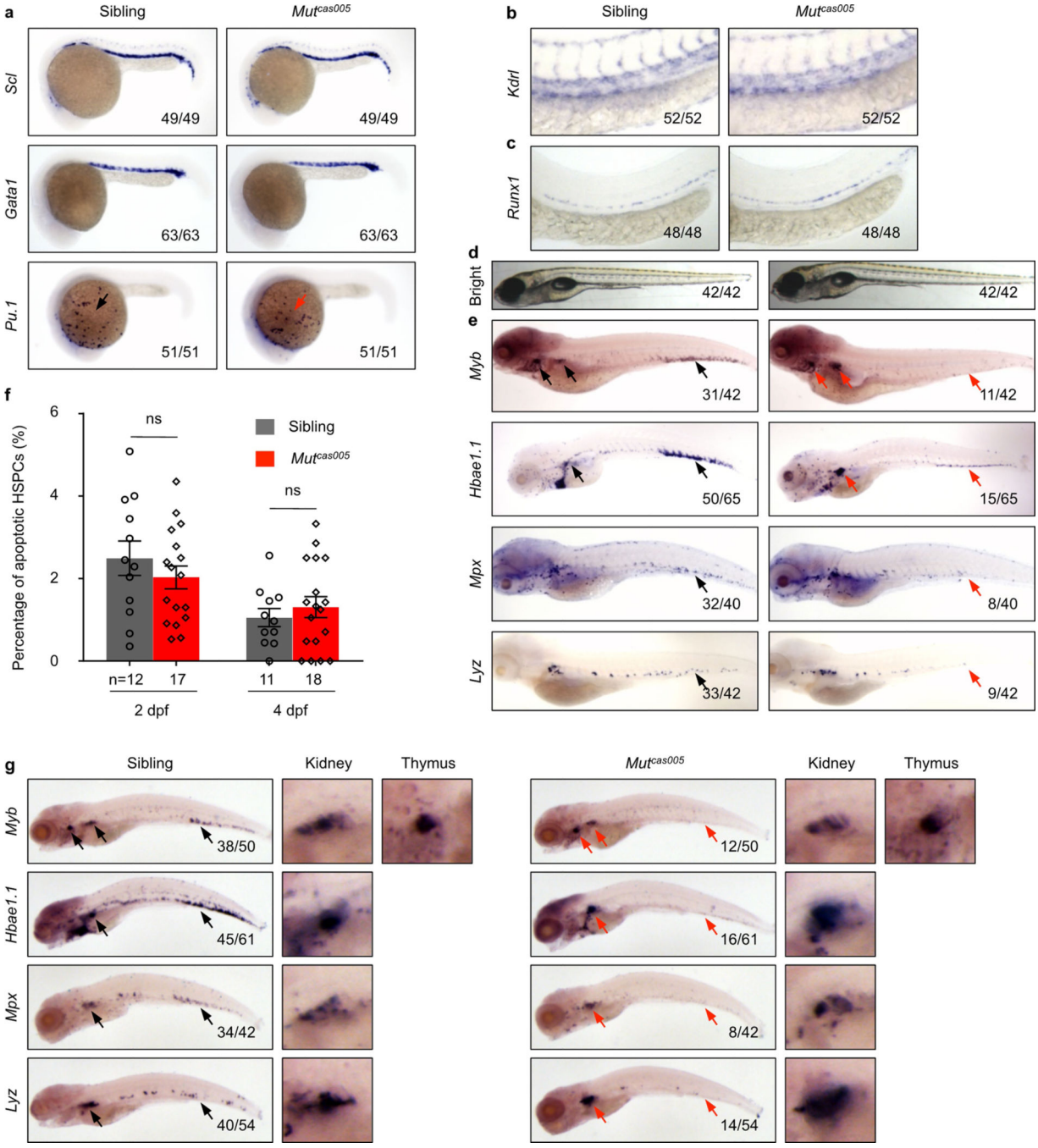

Extended Data Fig. 1 |. Phenotype characterization of zebrafish *mutant*^{cas005}.

a, Normal primitive haematopoiesis is intact in *mut*^{cas005}. WISH results demonstrate that the expression of primitive haematopoietic cell markers is identical between siblings and *mut*^{cas005} embryos at 22 h.p.f., including *scl* (also known as *tal1;* haematopoietic progenitor marker), *gata1* (also known as *gata1a;* erythrocyte progenitor marker) and *pu.1* (also known as *spi1b;* myeloid progenitor marker). **b,** The vascular development is normal in *mut*^{cas005} embryos. WISH results show no difference in the expression of *kdrl* (pan-endothelial cell marker) at 36 h.p.f. between wild-type siblings and *mut*^{cas005} embryos. **c,** The haemogenic

Author Manuscript Author Manuscript Author Manuscript Author Manuscript

endothelium is intact in *mut*^{cas005} embryos. WISH results show no difference in *runx1* expression at 36 h.p.f. in wild-type and *mut*^{cas005} embryos. **d, e,** The definitive haematopoiesis is defective in zebrafish *mut*^{cas005} embryos. **d,** Bright-field images of wild-type and *mut*^{cas005} embryos show no obvious morphological difference at 5 d.p.f. **e,** WISH results of *myb, hbae1.1, mpx* and *lyz* expression in wild-type and *mut*^{cas005} embryos at 5 d.p.f. Arrows indicate the comparable position in wild-type (black) or *mut*^{cas005} embryos (red). In 5 d.p.f. wild-type embryos, *myb* was expressed in all haematopoietic tissues including the CHT, thymus and kidney, whereas homozygous *mut*^{cas005} embryos displayed markedly decreased *myb* expression in the CHT, but similar expression to wild-type embryos in the thymus and kidney marrow. In accordance, the expression of downstream haematopoietic lineage cell markers, including *hbae1.1* (erythrocyte marker), *mpx* (granulocyte marker) and *lyz* (macrophage marker), also showed similar expression patterns in the wildtype (black) and *mut*^{cas005} (red) embryos to that of the *myb* WISH analysis. **f,** The percentage of apoptotic HSPCs detected by the TUNEL assay in 2 and 4 d.p.f. wild-type and *mut*^{cas005} embryos. 2 d.p.f.: $P = 0.35$, $t = 0.96$, df = 27; 4 d.p.f.: $P = 0.50$, $t = 0.69$, df = 27. Error bars denote s.e.m. **g,** At 7 d.p.f., *myb* expression in the thymus and kidney marrow was identical in wild-type sibling and *mut*^{cas005} embryos, whereas *mut*^{cas005} embryos still displayed markedly decreased *myb* expression in the CHT. In addition, *mut*^{cas005} embryos displayed notably decreased *hbae1.1, mpx* and *lyz* expression in the CHT but not in the kidney marrow.

Author Manuscript Author Manuscript Author Manuscript Author Manuscript

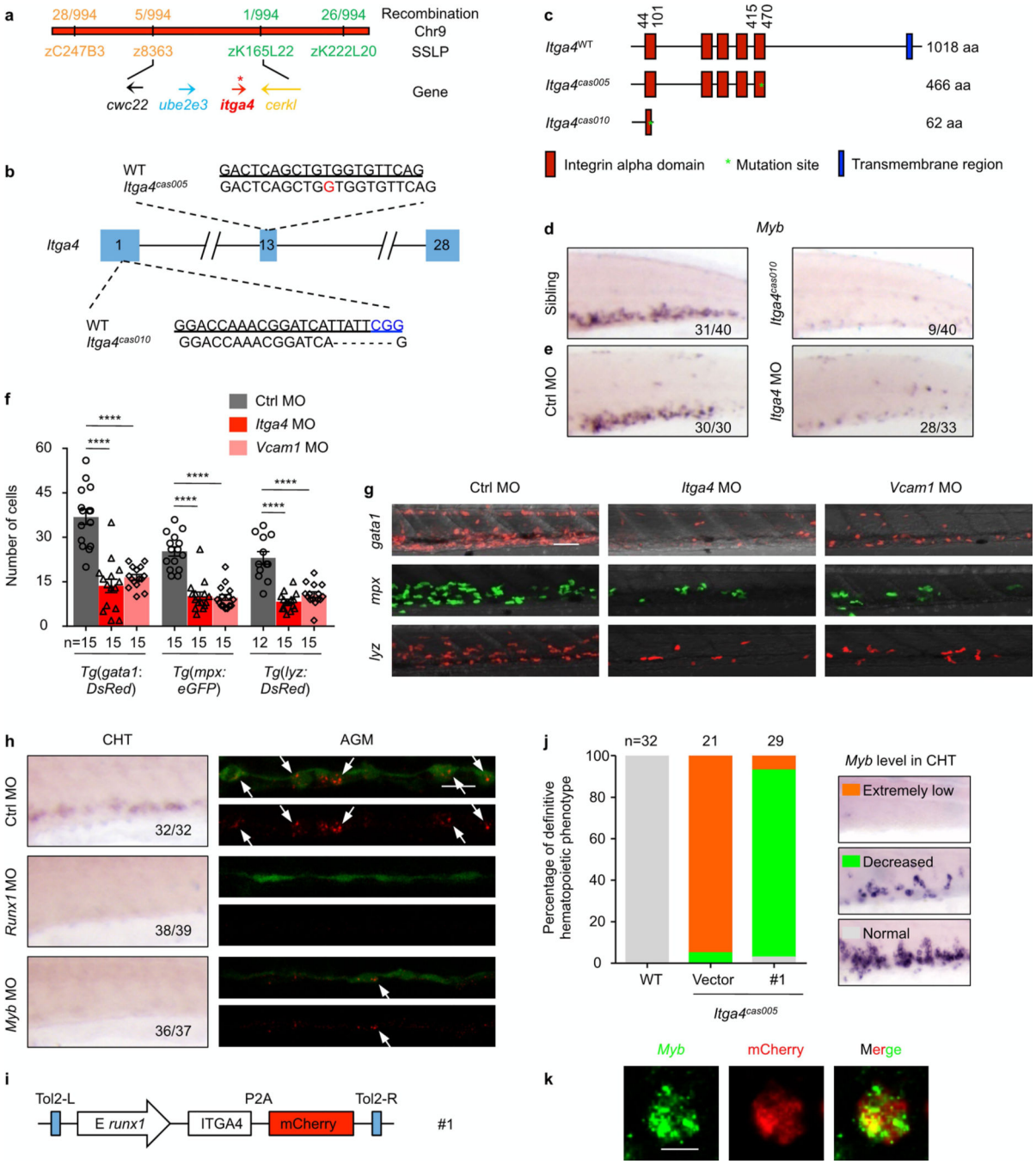

Extended Data Fig. 2 |. Genetic mapping and verification of zebrafish *itga4* mutants.

a, Positional cloning of *mut*^{cas005}. After high-resolution mapping, the point mutation is flanked by the SSLP markers z8363 (5 recombinant out of 994 meiosis) and zK165L22 (1 recombinant out of 994 meiosis). This region contains the four genes *cwc22, ube2e3, itga4* and *cerkl.* The red strip represents chromosome 9; the positions and recombination of the SSLP markers are indicated. SSLP markers on the same side of the mutation site are shown in the same colour. **b,** Generation of *itga4* mutants via the ENU(top) or CRISPR-Cas9 (bottom) technique. The alignment of wild-type (underlined) and mutated sequences is

Author Manuscript Author Manuscript Author Manuscript Author Manuscript

listed. The insertion in ENU is indicated in red (an insertion of G leading to an earlier stop codon in the *itga4* gene in *mut*^{cas005}*).* The PAM sequence of gRNA is 'CGG' (blue). Deletions are indicated by dashes. **c,** According to the stop codon in the genome of *itga4* mutants, SMART software was used to predict the structure of the wild-type *itga4,* *itga4*^{cas005} and *itga4*^{cas010} presumed protein. The molecular sizes of the presumed protein are indicated. **d,** The *myb* WISH results in wild-type and *itga4*^{cas010} embryos at 72 h.p.f. **e,** *itga4* morphants could phenocopy *itga4*^{cas005}. The validated *itga4* morpholino oligonucleotide (MO) that can block the translation of *itga4* mRNA was injected into one-cell-stage wild-type embryos to produce *itga4* morphants. WISH results of *myb* expression in the control and *itga4* morphants at 72 h.p.f. **f, g,** Representative live imaging (**g**) and statistical analysis (**f**) of *Tg(gata1:DsRed), Tg(mpx:eGFP)* and *Tg(lyzDsRed)* transgenic embryos after the injection of control or *itga4* or *vcam1* morpholino oligonucleotides at 84 h.p.f. Results show that downstream haematopoietic lineages were all defective owing to disrupted HSPC retention in the CHT. *gata1,* control vs *itga4* MO: ****$P < 0.0001$, $t = 7.42$, df = 14; *gata1,* control vs *vcam1* MO: ****$P < 0.0001$, $t = 8.11$, df = 14; *mpx,* control vs *itga4* MO: $P < 0.0001$, $t = 5.92$, df = 14; *mpx,* control vs *vcam1* MO: ****$P < 0.0001$, $t = 9.41$, df = 14; *lyz,* control vs *itga4* MO: ****$P < 0.0001$, $t = 7.16$, df = 25; *lyz,* control vs *vcam1* MO: ****$P < 0.0001$, $t = 5.74$, df = 25. **h,** In situ analysis of *itga4* expression in the AGM (FISH, 36 h.p.f.) and CHT (WISH, 72 h.p.f.) of *Tg(kdrl:eGFP)* (green) embryos after injection of control, *runx1* or *myb* morpholino oligonucleotides indicates HSPC cell-autonomous expression. **i-k,** *itga4* has an HSPC intrinsic mechanism during definitive haematopoiesis. **i,** The construction of the plasmid that was applied in the *itga4*^{cas005} mutant for Tol2-transposase-mediated transient transgenesis of *runx1*-enhancer-driven wild-type *itga4* expression. **j, k,** Phenotype analysis by *myb* WISH shows that the construct had a notable rescue effect on definitive haematopoiesis in the *itga4*^{cas005} mutant at 72 h.p.f. More than 45% of mCherry^{+} cells overlapped with *myb* FISH signalling in the CHT; a representative image is shown in **k**. Error bars denote s.e.m. Scale bars, 50 μm (**g**), 20 μm (**h**) and 5 μm (**k**).

Author Manuscript Author Manuscript Author Manuscript Author Manuscript

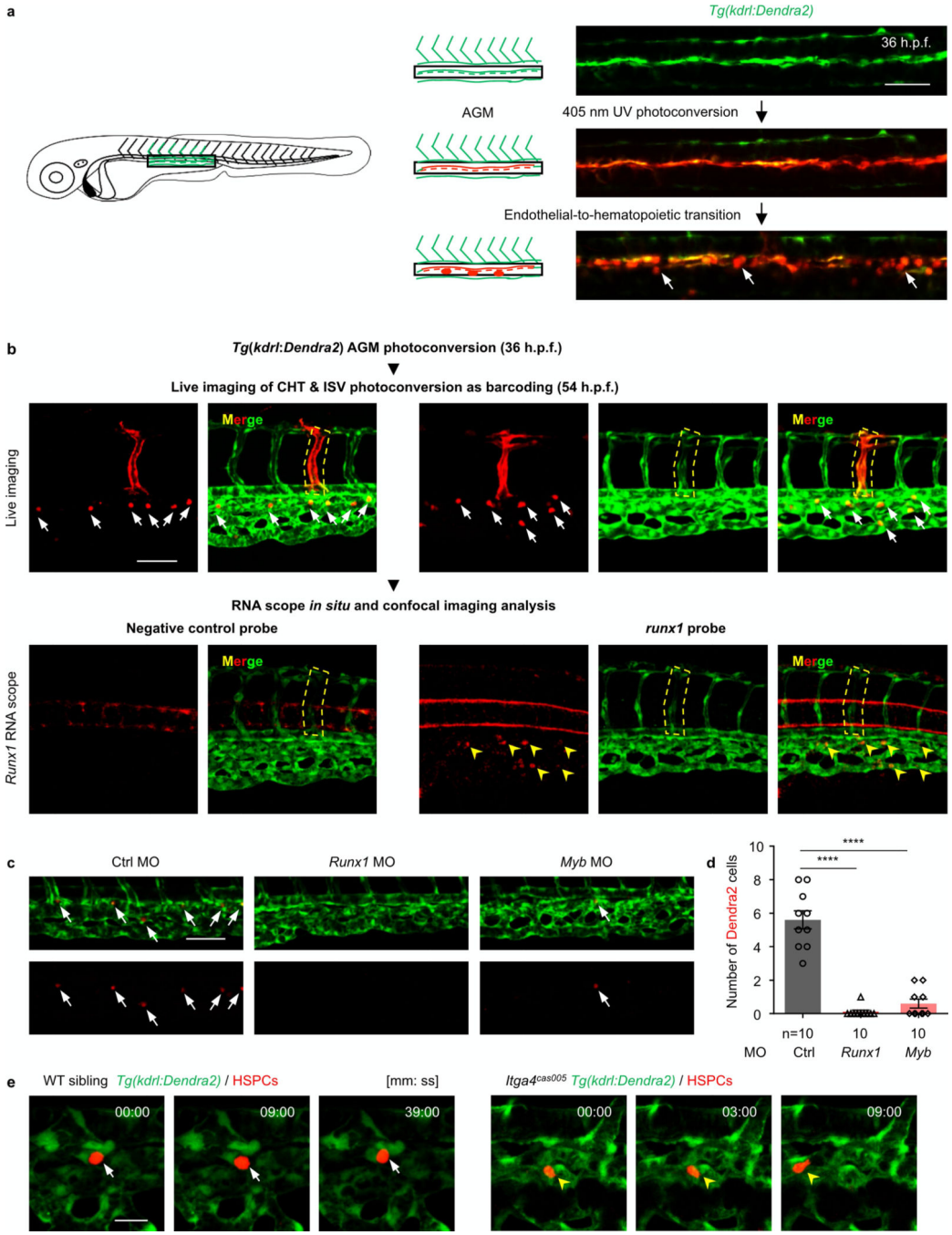

Extended Data Fig. 3 |. Photoconversion of *Tg(kdrl:Dendra2)* cells in the AGM can specifically mark HSPCs in the CHT.

a, Schematic illustration (left) and confocal imaging analysis (right) of the HSPC labelling system in live *Tg(kdrl:Dendra2)* transgenic zebrafish larva. At 32–36 h.p.f., an ultraviolet laser was applied to photoconvert Dendra2 in haemogenic endothelium from green to red fluorescence in the area marked by the rectangle. Endothelial-to-haematopoietic transition was observed with egress of single red Dendra2^{+} cells (white arrows) from the aortic ventral wall into the sub-aortic space. **b,** Flow chart of the experimental analysis on HSPCs (red

Author Manuscript Author Manuscript Author Manuscript Author Manuscript

Dendra2^{+} cells) in live-imaging and confocal-imaging analysis after in situ RNA scope in identical locations. Green Dendra2 signalling could remain during the experiment, whereas red Dendra2 signalling could not (the red fluorescence of the ISV disappeared after in situ RNA scope analysis). Photoconverting the ISV in different embryos makes each embryo distinguishable. (We distinguished the embryos by the position of the photoconverted and weakened Dendra2 green ISV). After live imaging the red Dendra2^{+} cells in the CHT (top, arrows) at 54 h.p.f., the embryos were fixed immediately for *runx1* in situ RNA scope analysis (bottom, yellow arrowheads). All HSPCs (red Dendra2^{+} cells) carry *runx1* transcripts, whereas there was no signal in the negative control. **c, d,** Confocal images of the CHT (c) and statistical analysis (**d**) at 54 h.p.f. show markedly reduced numbers of HSPCs (red Dendra2^{+} cells) in *runx1* and *myb* morphants, compared to that in control morphants. Control vs *runx1* MO: *****P* < 0.0001, $t = 9.15$, df = 9; control vs *myb* MO: *****P* < 0.0001, $t = 8.66$, df = 9. **e,** Live-imaging analysis on individual HSPCs in wild-type and itga4^{cas005} mutant embryos. Three representative frames from time-lapse imaging of 52–60 h.p.f. wild-type and *itga4*^{cas005} embryos with the *Tg(kdrl:Dendra2)* labelling system. The HSPCs (white arrow) remained stable in the vascular niche for over 30 min in the wild-type sibling (left); however, in the *itga4*^{cas005} mutants (right), the HSPCs (yellow arrowhead) remained for less than 9 min (see Supplementary Video 2). Error bars represent s.e.m. Scale bars, 50 μm (**a–c**) and 20 μm (**e**).

Author Manuscript Author Manuscript Author Manuscript Author Manuscript

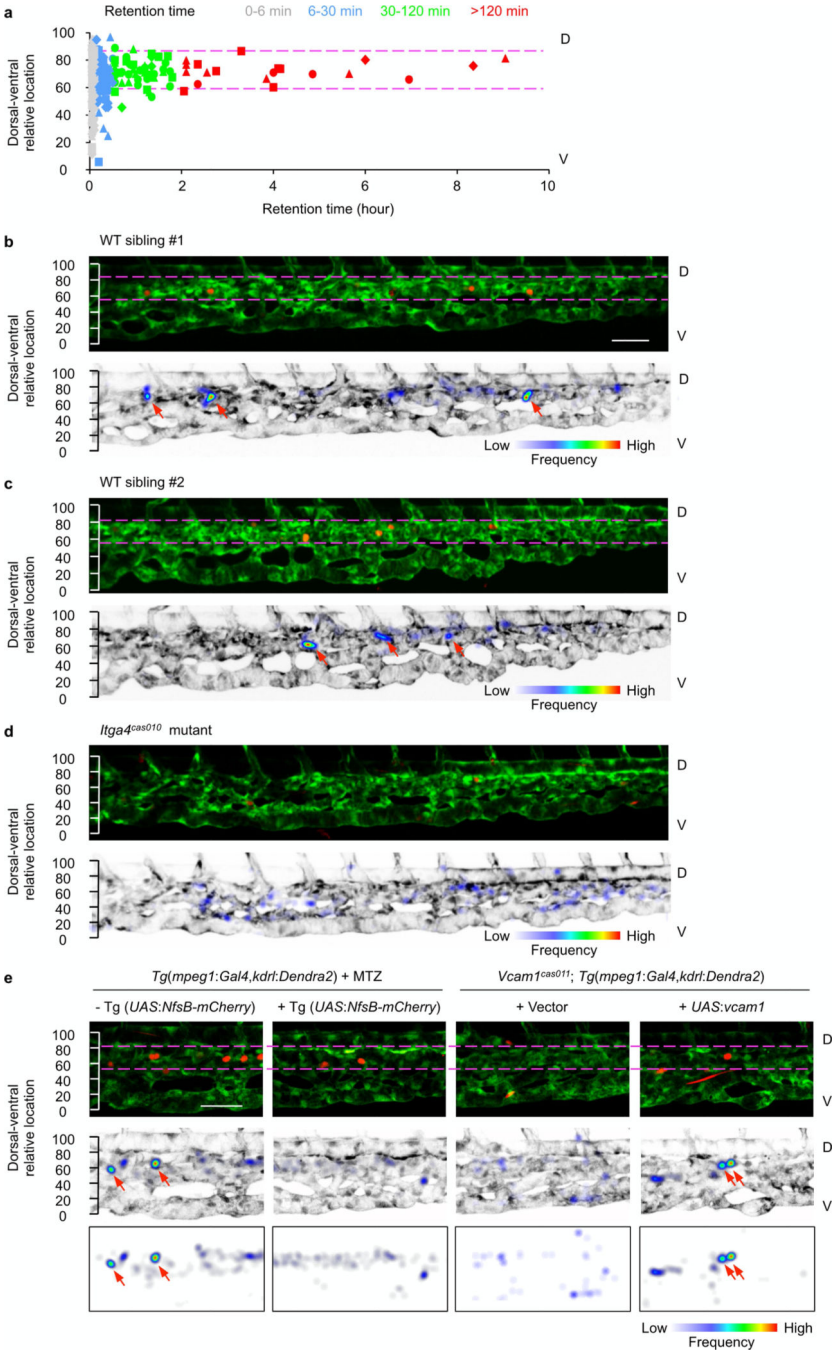

Extended Data Fig. 4 |. The HSPCs' retention 'hotspot' in the CHT.

a, Correlation analysis of retention time and the dorsal-ventral relative location of individual HSPCs in the CHT of four wild-type embryos at 50–60 h.p.f. Each shape represents one embryo (triangle, circle, square and rhombus), and each colour represent one class of retention time zone. HSPCs that remained for longer than 30 min were preferentially located in the region between the two magenta dashed lines enriched with venous capillaries. **b–d,** Longitudinal whole-mount images of the CHT in wild-type siblings (**b, c**) and *itga4*^{cas010} mutant embryos (**d**) in a *Tg(kdrl:Dendra2)* background after photoconversion and retention

Author Manuscript Author Manuscript Author Manuscript Author Manuscript

calculation of the frequency of HSPC appearance. **e,** Longitudinal whole-mount images of the CHT in *Tg(mpeg1:Gal4,kdrl:Dendra2)* embryos after MTZ treatment with or without a *Tg(UASNfsB-mCherry)* background, and *vcam1*^{cas011}*; Tg(mpeg1:Gal4,kdrl:Dendra2)* embryos with transient transgenesis of vector *(UAS:polyA)* or *UAS:vcam1* after photoconversion and retention calculation of the frequency of HSPC appearance. Red arrows denote retention hotspots. HSPCs were preferentially located in the region between the two magenta dashed lines. Retention hotspots disappeared in the *itga4*^{cas010}and *vcam1*^{cas011} mutants after depletion of macrophages (MTZ treatment on NfsB-expressing macrophages). Scale bars, 50 μm.

Author Manuscript Author Manuscript Author Manuscript Author Manuscript

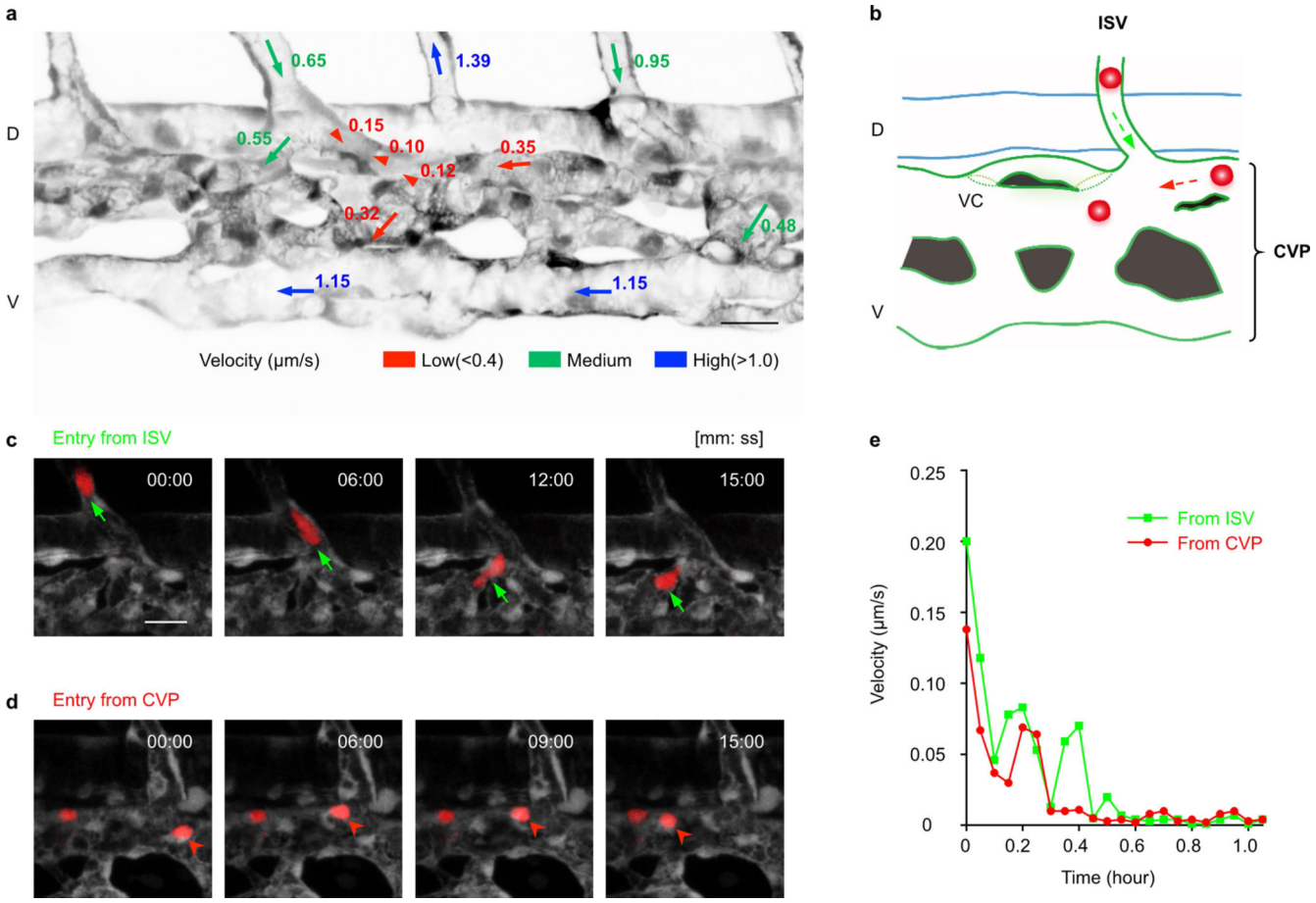

Extended Data Fig. 5 |. HSPCs decelerate in the CHT vascular niche.

a, Representative spatial maps of the flow velocity of photoconverted HSPCs in the caudal vasculature at 54 h.p.f. Arrows show the direction of blood flow, and different colours indicate the level of velocity. **b,** Schematic illustration of how HSPCs enter the CHT via the circulation. **c–e,** Time-lapse imaging (**c, d**) and speed curve diagram (**e**) show that HSPCs arrive either from the intersegmental vessel (green arrow in **c**) or the CVP (red arrowhead in **d**) into the CHT and gradually decelerate (see Supplementary Video 3). Scale bar, 20 μm.

Author Manuscript Author Manuscript Author Manuscript Author Manuscript

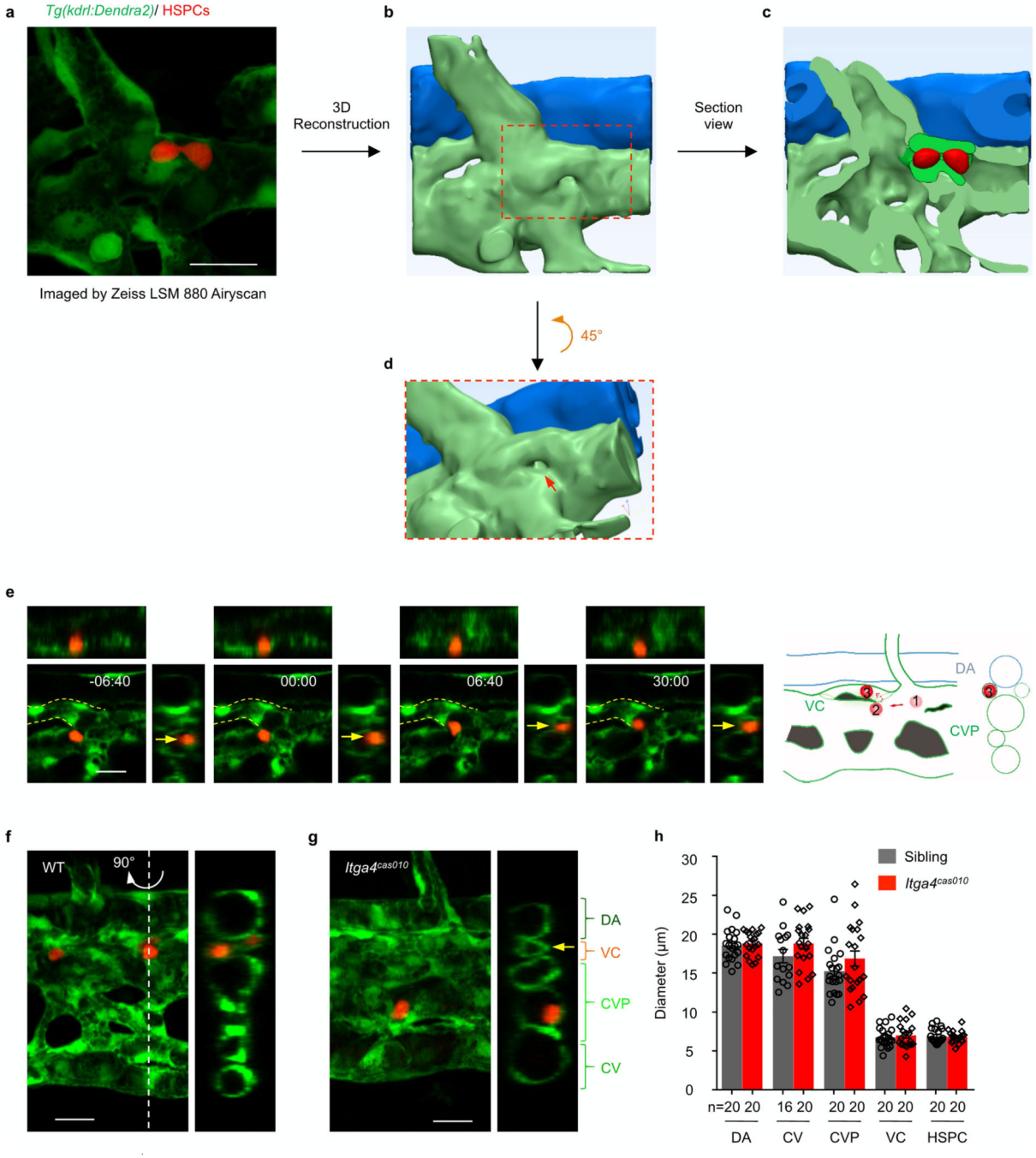

Extended Data Fig. 6 |. The representative high-resolution vascular structure and HSPC in the retention hotspot.

a, The original fluorescent image of the vessel surrounding HSPCs in the retention hotspot was captured by an LSM880 microscope equipped with Airyscan function and processed by 3D reconstruction (see Supplementary Video 4). **b,** 3D reconstruction of **a. c,** Section view of the caudal vein plexus and capillary. **d,** The 45° rotation view of the red frame in **b. e,** Time-lapse imaging (left) and scheme graph (right) show how HSPC retention occurs. HSPCs initially came into the venous plexus and then entered the venous capillary for long-

Author Manuscript Author Manuscript Author Manuscript Author Manuscript

term retention. **f–h,** Images (**f, g**) and statistical analysis (**h**) show that the diameter of various vessels in the CHT in *itga4*^{cas010} mutants (**g**) is similar to that in the wild-type siblings (**f**) at 54 h.p.f. The inner diameter of venous capillaries, but not other vessels, is close to the diameter of HSPCs. DA: $P = 0.73$, $t = 0.35$, df = 19; CV: $P = 0.14$, $t = 1.52$, df = 33; CVP: $P = 0.17$, $t = 1.41$, df = 19; VC: $P = 0.63$, $t = 0.49$, df = 19; HSPC: $P = 0.67$, $t = 0.44$, df = 19. Scale bar, 20 μm.

Author Manuscript Author Manuscript Author Manuscript Author Manuscript

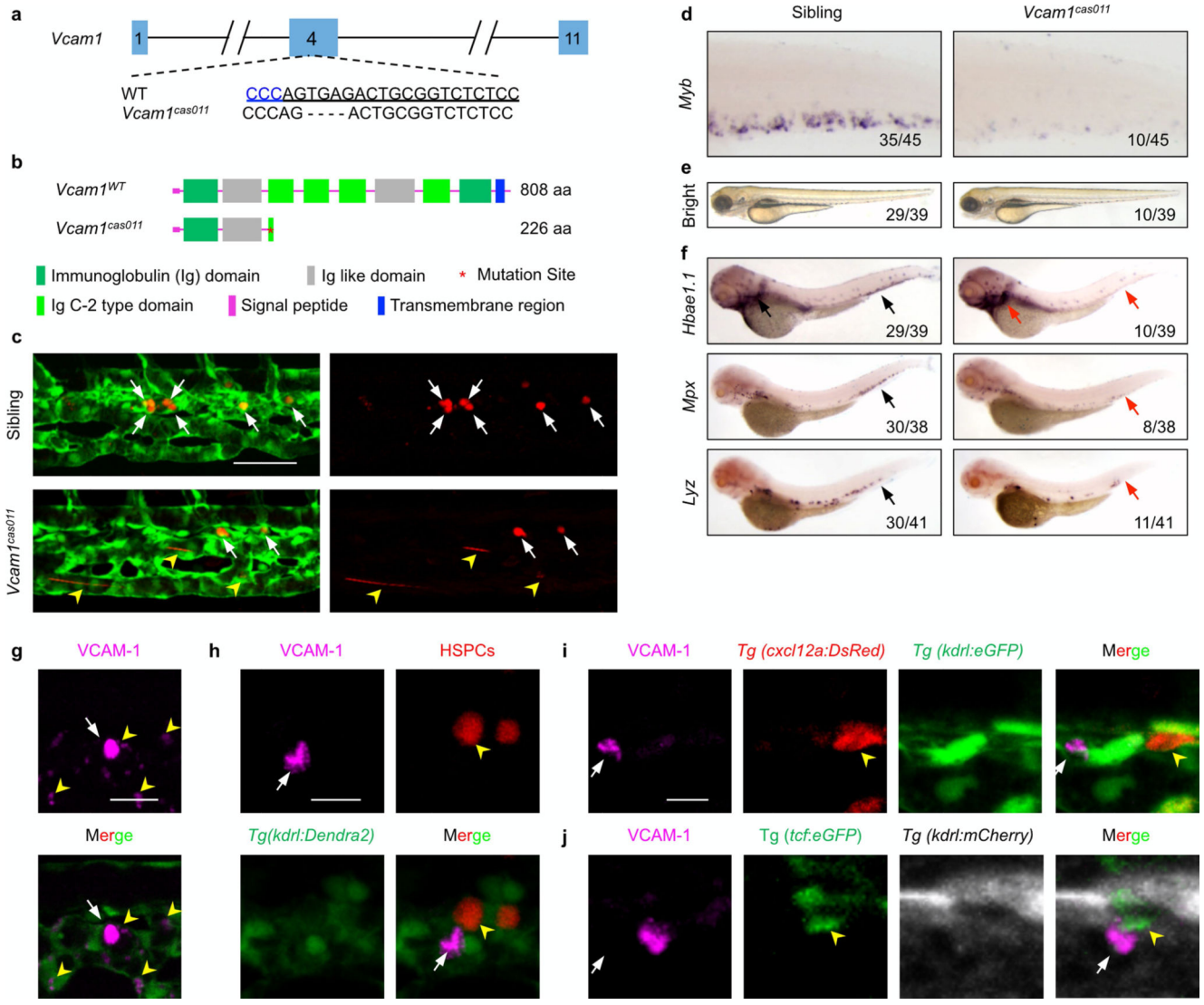

Extended Data Fig. 7 |. Characterization of VCAM-1^{+} cells in the CHT.

a, Generation of the *vcaml* mutant using the CRISPR-Cas9 technique. The alignment of wild-type (underlined) and mutated sequences is listed. The PAM sequence of gRNA is 'GGG' (in blue). Deletions are indicated by dashes. **b,** According to the stop codon in the genome, SMART software was used to predict the structure of the wild-type *vcaml* and *vcam1*^{cas011} presumed protein. The molecular sizes of the presumed protein are indicated. **c,** Live imaging of the CHT at 54 h.p.f. shows retention defects in *vcam1*^{cas011} mutants. Representative images show that most HSPCs resided within the CHT (white arrows) in wild-type siblings (top), whereas these cells went through quickly in *vcam1*^{cas011} embryos (bottom, yellow arrowheads) (see Supplementary Video 5). **d,** WISH analysis of *myb* expression in the CHT of wild-type and *vcam1*^{cas011} embryos at 72 h.p.f. **e, f,** The definitive haematopoiesis is defective in *vcam1*^{cas011} mutant zebrafish embryos. **e,** The bright-field images of wild-type and *vcam1*^{cas011} embryos show no obvious morphological difference at 72 h.p.f. **f,** WISH results of *hbael.1, mpx* and *lyz* expression in wild-type and *vcam1*^{cas011} mutant embryos at 72 h.p.f. Arrows indicate the comparable position in wild-type (black) or

Author Manuscript Author Manuscript Author Manuscript Author Manuscript

vcam1^{cas011} (red) embryos. **g,** Magnified views showed VCAM-1 was mainly expressed in individual cells (white arrow) but weakly expressed on the venous endothelial cells (yellow arrowheads). **h,** After photoconversion, *Tg(kdrl:Dendra2)* embryos are stained with anti-VCAM-1 (magenta, white arrow). The yellow arrowhead denotes an HSPC. **i,** *Tg(cxcl12a:DsRed,kdrl:eGFP)* transgenic embryos are stained with anti-VCAM-1 (magenta, white arrow) and anti-DsRed (red, yellow arrowhead). **j,** *Tg(tcf:eGFP,kdrl:mCherry)* transgenic embryos are stained with anti-VCAM-1 (magenta, white arrows) and anti-GFP (green, yellow arrowheads). Scale bars, 50 μm (**c**), 20 μm (**g**) and 10 μm (**h, i**).

Author Manuscript Author Manuscript Author Manuscript Author Manuscript

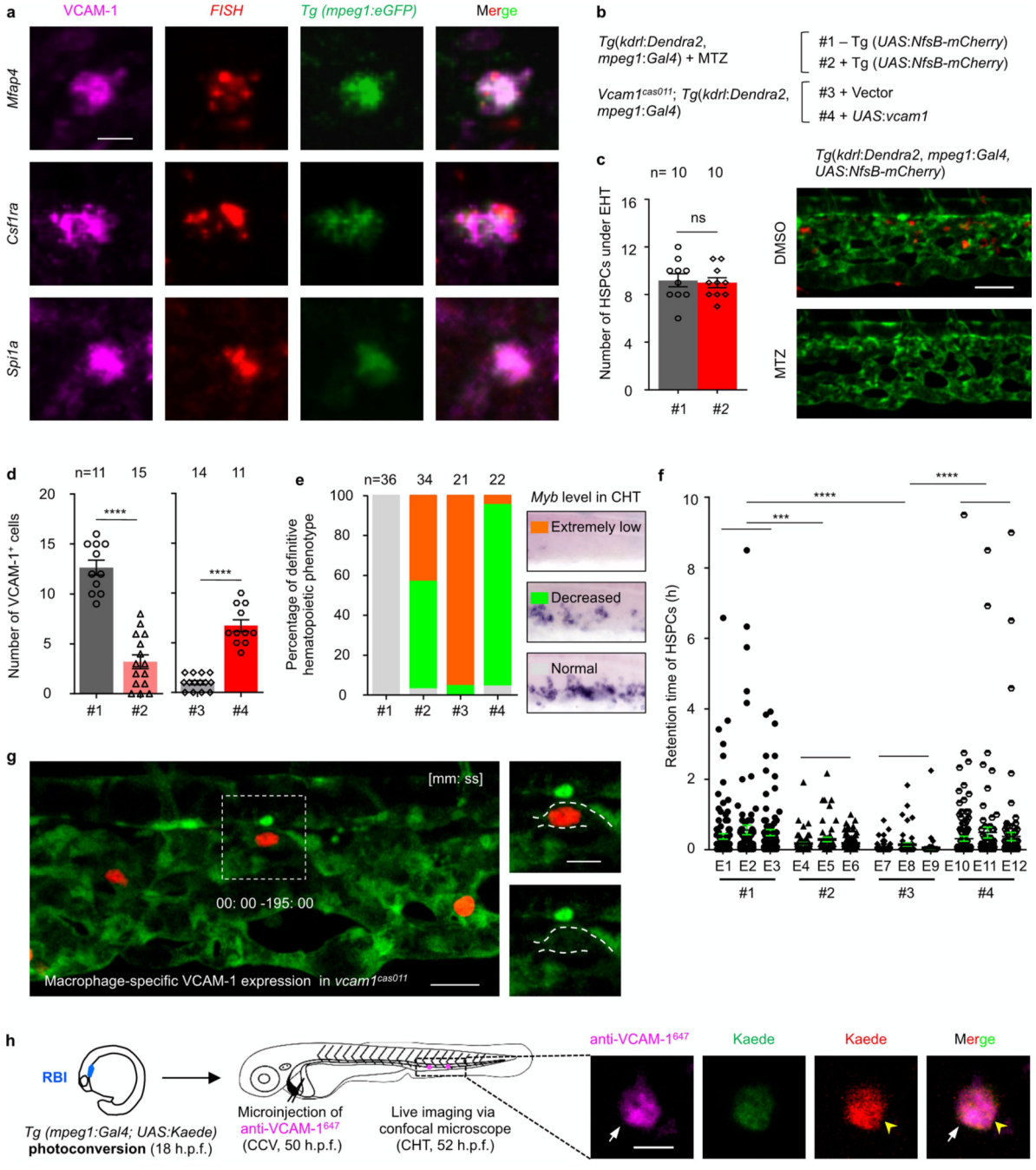

Extended Data Fig. 8 |. Distinct role of macrophages and venous endothelium VCAM-1 in HSPCs retention.

a, Representative FISH confocal imaging of *mfap4* (top), *csf1ra* (middle), *spi1a* (bottom) immunofluorescence with anti-VCAM-1 and anti-GFP antibodies indicates that VCAM-1^{+} cells in the CHT are macrophage-like cells (see Supplementary Table 2). **b,** The construction of the plasmid applied in **c–f. c,** Validation of the macrophage-specific cell-depletion system. Left, the number of HSPCs under the endothelial-to-haematopoietic transition (EHT) process in the AGM of *Tg(mpeg1:Gal4,kdrl:Dendra2)* transgenic embryos at 54 h.p.f. with

Author Manuscript Author Manuscript Author Manuscript Author Manuscript

MTZ treatment and with (#2) or without (#1) the *Tg(UAS:NfsB-mCherry)* background. $P = 0.80$, $t = 0.25$, df = 9. Right, live imaging of vessels (green) and macrophages (red) with or without MTZ treatment in the CHT of *Tg(kdrl:Dendra2,mpeg1:Gal4,UAS*:N *fsB-mCherry)* transgenic embryos showed that MTZ treatment could delete almost all mCherry^{+} macrophages. **d,** Quantification of VCAM-1^{+} cells in the CHT, detected by anti-VCAM-1 immunofluorescence, in *Tg(mpeg1:Gal4,kdrl:Dendra2)* embryos at 54 h.p.f. with MTZ treatment and with (#2) or without (#1) a *Tg(UAS:NfsB-mCherry)* background, and in *vcam1*^{cas011} mutants with Tol2-mediated transient transgenesis of vector *(UAS:polyA)* (#3) or *UAS:vcam1* (#4) in a *Tg(mpeg1:Gal4,kdrl:Dendra2)* background. #1 vs #2: $^{****}P < 0.0001$, $t = 9.18$, df = 24; #3 vs #4: $^{****}P < 0.0001$, $t = 10.03$, df = 23. **e,** Statistical analysis shows the percentage of the three types of definitive haematopoietic phenotype (extremely low, decreased or normal) in the four experimental conditions (#1-#4) linked to **d.** Macrophage-specific cell depletion caused deficient definitive haematopoiesis; however, macrophage-specific VCAM-1 re-expression markedly rescued deficient haematopoiesis in *vcam1*^{cas011} mutants. **f,** Retention time of individual HSPCs in transgenic *Tg(mpeg1:Gal4,kdrl:Dendra2)* embryos at 50–60 h.p.f. with MTZ treatment and with (#2) or without (#1) a *Tg(UAS:NfsB-mCherry)* background, and in *vcam1*^{cas011} mutants with Tol2-mediated transient transgenesis of vector (UAS*:polyA)* (#3) or *UAS:vcam1* (#4) in a *Tg(mpeg1:Gal4,kdrl:Dendra2)* background (see Fig. 2f, g). #1 vs #2: $^{***}P = 0.0001$, $t = 3.85$, df = 550; #1 vs #3: $^{****}P < 0.0001$, $t = 6.05$, df = 565; #3 vs #4: $^{****}P < 0.0001$, $t = 4.37$, df = 590. g, Live-imaging frame shots of HSPCs in which macrophage-specific VCAM-1 was in re-expressed *vcam1*^{cas011} mutants from Fig. 2g (see Supplementary Video 6). h, Schematic illustration shows that macrophage labelling (photoconverted Kaede^{+}; red) was performed at 18 h.p.f. in the rostral blood island (RBI) in *Tg(mpeg1:Gal4, UAS:Kaede)* embryos, followed by a 1 nl anti-VCAM-1^{647} (0.4 ng) antibody injection at 50 h.p.f. Cell-lineage tracing of the labelled macrophages (red; yellow arrowheads) in vivo was performed from 2 h after the injection. Representative images show that macrophages from the rostral blood island at 18 h.p.f. migrate to the CHT, and are VCAM-1^{+}. Scale bars, 50 μm (**c**), 20 μm (**g**), 10 μm (**h**) and 5 μm (**a**).

Author Manuscript Author Manuscript Author Manuscript Author Manuscript

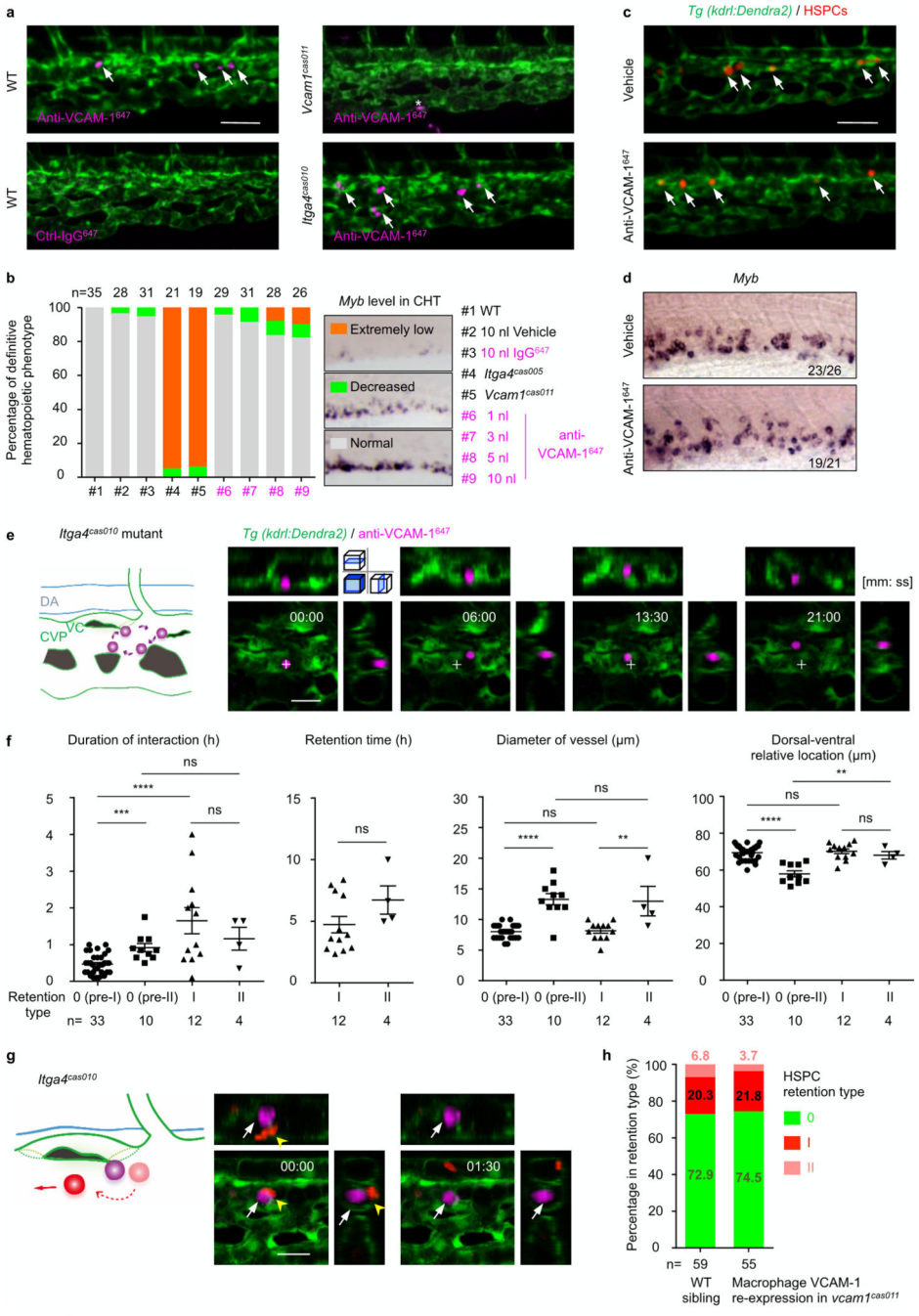

Extended Data Fig. 9 |. Anti-VCAM-1^{647} antibody labels usher cells without disrupting definitive haematopoiesis.

a, Injection of 1 nl (0.4 ng) of anti-VCAM-1^{647} antibody labels usher cells (arrows) in wildtype and *itga4*^{cas010} mutants in the *Tg(kdrl:eGFP)* background, whereas injection of either control (non-specific) IgG^{647} antibody into wildtype cells or anti-VCAM-1^{647} antibody into *vcam1*^{cas011} mutants in the *Tg(kdrl:eGFP)* background did not label any cells in the retention hotspots. Asterisk indicates nonspecific labelling on a chromatophore in the CHT. **b,** Anti-VCAM-1^{647} injection marginally influence definitive haematopoiesis.

Author Manuscript Author Manuscript Author Manuscript Author Manuscript

Statistical analysis shows the percentage of the three types of definitive haematopoietic phenotype in nine different conditions, including wild-type embryos without injection (#1), with 10 nl vehicle (#2) or 10 nl 0.4 mg ml^{-1} IgG^{647} injection (#3), *itga4*^{cas005} mutants (#4) or *vcam1*^{cas011} mutants (#5) without injection, and wild-type embryos with 1–10 nl 0.4 mg ml^{-1} anti-VCAM-1^{647} injection (#6-#9). **c, d,** Live imaging of HSPCs (**c**) or WISH analysis of the *myb* probe at 60 h.p.f. (**d**) of the wild-type CHT after vehicle or 1 nl anti-VCAM-1^{647} antibody injection. **e,** Schematic diagrams (left) and confocal imaging (right) show VCAM-1^{+} cells patrolling on a small scale in the CHT in *itga4*^{cas010} mutant embryos. Cross indicates the original position at the initial time point. **f,** Statistical analysis of the duration of the interaction between HSPCs and usher cells, the HSPC retention time, the diameter of vessels and the dorsal-ventral relative location for HSPC retention in pre-type I (type 0), pre-type II (type 0), type I and type II. Duration, pre-I vs pre-II: ***P = 0.0001, t = 4.25, df = 41; duration, pre-I vs I: ****P< 0.0001, t = 5.31, df = 43; duration, pre-II vs II: P = 0.37, t = 0.93, df = 12; duration, I vs II: P = 0.46, t = 0.76, df = 14; retention: P = 0.16, t = 1.50, df = 14; diameter, pre-I vs pre-II: ****P < 0.0001, t = 8.80, df = 41; diameter, pre-I vs I: P = 0.68, t = 0.42, df = 43; diameter, pre-II vs II: P = 0.89, t = 0.14, df = 12; diameter, I vs II: **P = 0.006, t = 3.24, df = 14; location, pre-I vs pre-II: ****P < 0.0001, t = 7.64, df = 41; location, pre-I vs I: P = 0.6, t = 0.53, df = 43; location, pre-II vs II: **P = 0.005, t = 3.41, df = 12; location, I vs II: P = 0.41, t = 0.85, df = 14. **g,** In *itga4*^{cas010} mutants, HSPCs encountered but failed to interact with usher cells and then went through the CHT within a few minutes (see Supplementary Video 10). **h,** The percentage of the type 0, type I and type II HSPC retention types in wild-type sibling and *vcam1*^{cas011} mutants in the *Tg(mpeg1:Gal4,kdrl:Dendra2)* background with transient transgenesis of *UAS:vcam1.* None of the HSPCs in the *vcam1* mutants could be classified into either type I or II retention types, or were comparable with the HSPCs in Extended Data Fig. 8h. Scale bars, 50 μm (**a, c**) and 20 μm (**e, g**).

Supplementary Material

Refer to Web version on PubMed Central for supplementary material.

Acknowledgements

We thank the following people for the zebrafish transgenic lines: L. Luo for *Tg(kdrl:Dendra2),* Z. Wen for *Tg(mpeg1:Gal4,UAS:NfsB-mCherry), Tg(UASKaede)* and *Tg(mpeg1:eGFP),* B. Blazar for *Tg(cxcl12a:dsRed)* and F. Argenton for *Tg(tcf:eGFP).* We are also grateful to M. Deng and J. He for technical support, and Z. Wen, L. Li, L. Zon, J. Peng and A. Meng for discussions. This work was granted by CAS Strategic Priority Research Program (XDB19030000), Ministry of Science and Technology of China (2017YF0503600), National Natural Science Foundation of China (31571505 and 31371461), CAS Scientific Research Equipment Development Project (YZ201646) and Science and Technology Commission of Shanghai Municipality (13JC1406400) to W.J.P.

References

1. Morrison SJ, Uchida N & Weissman IL The biology of hematopoietic stem cells. Annu. Rev. Cell Dev. Biol 11, 35–71 (1995). [PubMed: 8689561]
2. Murayama E et al. Tracing hematopoietic precursor migration to successive hematopoietic organs during zebrafish development. Immunity 25, 963–975 (2006). [PubMed: 17157041]
3. Kissa K & Herbomel PBlood stem cells emerge from aortic endothelium by a novel type of cell transition. Nature 464, 112–115 (2010). [PubMed: 20154732]

Author Manuscript Author Manuscript Author Manuscript Author Manuscript

4. Bertrand JY et al. Haematopoietic stem cells derive directly from aortic endothelium during development. Nature 464,108–111 (2010). [PubMed: 20154733]
5. Boisset JC et al. In vivo imaging of haematopoietic cells emerging from the mouse aortic endothelium. Nature 464, 116–120 (2010). [PubMed: 20154729]
6. Xue Y et al. The vascular niche regulates hematopoietic stem and progenitor cell lodgment and expansion via klf6a-ccl25b. Dev. Cell 42, 349–362.e4 (2017). [PubMed: 28803829]
7. Mahony CB, Fish RJ, Pasche C & Bertrand JY tfec controls the hematopoietic stem cell vascular niche during zebrafish embryogenesis. Blood 128, 1336–1345 (2016). [PubMed: 27402973]
8. Glass TJ et al. Stromal cell-derived factor-1 and hematopoietic cell homing in an adult zebrafish model of hematopoietic cell transplantation. Blood 118, 766–774 (2011). [PubMed: 21622651]
9. Murayama E et al. NACA deficiency reveals the crucial role of somite-derived stromal cells in haematopoietic niche formation. Nat. Commun 6, 8375 (2015). [PubMed: 26411530]
10. Jin H, Xu J & Wen Z Migratory path of definitive hematopoietic stem/progenitor cells during zebrafish development. Blood 109, 5208–5214 (2007). [PubMed: 17327398]
11. Burns CE, Traver D, Mayhall E, Shepard JL & Zon LI Hematopoietic stem cell fate is established by the Notch-Runx pathway. Genes Dev. 19, 2331–2342 (2005). [PubMed: 16166372]
12. Jao LE, Wente SR & Chen W Efficient multiplex biallelic zebrafish genome editing using a CRISPR nuclease system. Proc. Natl Acad. Sci. USA 110, 13904–13909 (2013). [PubMed: 23918387]
13. Soza-Ried C, Hess I, Netuschil N, Schorpp M & Boehm T Essential role of c-myb in definitive hematopoiesis is evolutionarily conserved. Proc. Natl Acad. Sci. USA 107, 17304–17308 (2010). [PubMed: 20823231]
14. Tamplin OJ et al. Hematopoietic stem cell arrival triggers dynamic remodeling of the perivascular niche. Cell 160, 241–252 (2015). [PubMed: 25594182]
15. Arroyo AG, Yang JT, Rayburn H & Hynes RO a4 integrins regulate the proliferation/differentiation balance of multilineage hematopoietic progenitors in vivo. Immunity 11, 555–566 (1999). [PubMed: 10591181]
16. Imai Y, Shimaoka M & Kurokawa M Essential roles of VLA-4 in the hematopoietic system. Int. J. Hematol. 91, 569–575 (2010). [PubMed: 20352381]
17. Gribi R, Hook L, Ure J & Medvinsky A The differentiation program of embryonic definitive hematopoietic stem cells is largely a4 integrin independent. Blood 108, 501–509 (2006). [PubMed: 16551970]
18. Qian H et al. Distinct roles of integrins a6 and a4 in homing of fetal liver hematopoietic stem and progenitor cells. Blood 110, 2399–2407 (2007). [PubMed: 17586725]
19. Scott LM, Priestley GV & Papayannopoulou T Deletion of α4 integrins from adult hematopoietic cells reveals roles in homeostasis, regeneration, and homing. Mol. Cell. Biol 23, 9349–9360 (2003). [PubMed: 14645544]
20. Nombela-Arrieta C et al. Quantitative imaging of haematopoietic stem and progenitor cell localization and hypoxic status in the bone marrow microenvironment. Nat. Cell Biol. 15, 533–543 (2013). [PubMed: 23624405]
21. Osborn L et al. Direct expression cloning of vascular cell adhesion molecule 1, a cytokine-induced endothelial protein that binds to lymphocytes. Cell 59, 1203–1211 (1989). [PubMed: 2688898]
22. Elices MJ et al. VCAM-1 on activated endothelium interacts with the leukocyte integrin VLA-4 at a site distinct from the VLA-4/fibronectin binding site. Cell 60, 577–584 (1990). [PubMed: 1689216]
23. Koenig JM, Ballantyne CM, Kumar AG, Smith CW & Yoder MC Vascular cell adhesion molecule-1 expression and hematopoietic supportive capacity of immortalized murine stromal cell lines derived from fetal liver and adult bone marrow. In Vitro Cell. Dev. Biol. Anim 38, 538–543 (2002). [PubMed: 12703982]
24. Berlin C et al. a4 integrins mediate lymphocyte attachment and rolling under physiologic flow. Cell 80, 413–422 (1995). [PubMed: 7532110]
25. Warga RM, Kane DA & Ho RK Fate mapping embryonic blood in zebrafish: multi- and unipotential lineages are segregated at gastrulation. Dev. Cell 16, 744–755 (2009). [PubMed: 19460350]

Author Manuscript Author Manuscript Author Manuscript Author Manuscript

26. Winkler IG et al. Bone marrow macrophages maintain hematopoietic stem cell (HSC) niches and their depletion mobilizes HSCs. Blood 116, 4815–4828 (2010). [PubMed: 20713966]
27. Dutta P et al. Macrophages retain hematopoietic stem cells in the spleen via VCAM-1. J. Exp. Med 212, 497–512 (2015). [PubMed: 25800955]
28. Jin H et al. Definitive hematopoietic stem/progenitor cells manifest distinct differentiation output in the zebrafish VDA and PBI. Development 136, 647–654 (2009). [PubMed: 19168679]
29. Traver D et al. Transplantation and in vivo imaging of multilineage engraftment in zebrafish bloodless mutants. Nat. Immunol 4, 1238–1246 (2003). [PubMed: 14608381]
30. Shi X et al. Functions of idhl and its mutation in the regulation of developmental hematopoiesis in zebrafish. Blood 125, 2974–2984 (2015). [PubMed: 25778530]
31. Hall C, Flores MV, Storm T, Crosier K & Crosier P The zebrafish lysozyme C promoter drives myeloid-specific expression in transgenic fish. BMC Dev. Biol 7 42 (2007). [PubMed: 17477879]
32. Liu C et al. Macrophages mediate the repair of brain vascular rupture through direct physical adhesion and mechanical traction. Immunity 44, 1162–1176 (2016). [PubMed: 27156384]
33. Cross LM, Cook MA, Lin S, Chen JN & Rubinstein AL Rapid analysis of angiogenesis drugs in a live fluorescent zebrafish assay. Arterioscler. Thromb. Vasc. Biol 23, 911–912 (2003). [PubMed: 12740225]
34. Davison JM et al. Transactivation from Gal4-VP16 transgenic insertions for tissue-specific cell labeling and ablation in zebrafish. Dev. Biol 304, 811–824 (2007). [PubMed: 17335798]
35. Scott EK & Baier H The cellular architecture of the larval zebrafish tectum, as revealed by Gal4 enhancer trap lines. Front. Neural Circuits 3, 13 (2009). [PubMed: 19862330]
36. Moro E et al. In vivo Wnt signaling tracing through a transgenic biosensor fish reveals novel activity domains. Dev. Biol 366, 327–340 (2012). [PubMed: 22546689]
37. Ellett F, Pase L, Hayman JW, Andrianopoulos A & Lieschke GJ mpegl promoter transgenes direct macrophage-lineage expression in zebrafish. Blood 117, e49–e56 (2011). [PubMed: 21084707]
38. Bahary N et al. The Zon laboratory guide to positional cloning in zebrafish. Methods Cell Biol. 77, 305–329 (2004). [PubMed: 15602919]
39. Knapik EW et al. A microsatellite genetic linkage map for zebrafish (Danio rerio). Nat. Genet 18, 338–343 (1998). [PubMed: 9537415]
40. Scheer N & Campos-Ortega JA Use of the Gal4-UAS technique for targeted gene expression in the zebrafish. Mech. Dev 80, 153–158 (1999). [PubMed: 10072782]
41. Lam EYN et al. Zebrafish runxl promoter-EGFP transgenics mark discrete sites of definitive blood progenitors. Blood 113, 1241–1249 (2009). [PubMed: 18927441]
42. Nasevicius A & Ekker SC Effective targeted gene ‘knockdown’ in zebrafish. Nat. Genet 26, 216–220 (2000). [PubMed: 11017081]
43. Suster ML, Kikuta H, Urasaki A, Asakawa K & Kawakami K Transgenesis in zebrafish with the Tol2 transposon system. Methods Mol. Biol 561, 41–63 (2009). [PubMed: 19504063]
44. Xiao A et al. Chromosomal deletions and inversions mediated by TALENs and CRISPR/Cas in zebrafish. Nucleic Acids Res. 41, e141 (2013). [PubMed: 23748566]
45. Gao L et al. TopBP1 governs hematopoietic stem/progenitor cells survival in zebrafish definitive hematopoiesis. PLoS Genet. 11, e1005346 (2015). [PubMed: 26131719]
46. Patterson LJ et al. The transcription factors Scl and Lmo2 act together during development of the hemangioblast in zebrafish. Blood 109, 2389–2398 (2007). [PubMed: 17090656]
47. Jia XE et al. Mutation of krill causes definitive hematopoiesis failure via PERK-dependent excessive autophagy induction. Cell Res. 25, 946–962 (2015). [PubMed: 26138676]
48. Zakrzewska A et al. Macrophage-specific gene functions in Spi1-directed innate immunity. Blood 116, e1–e11 (2010). [PubMed: 20424185]
49. Jowett T & Lettice L Whole-mount in situ hybridizations on zebrafish embryos using a mixture of digoxigenin- and fluorescein-labelled probes. TIG 10, 73–74 (1994). [PubMed: 8178366]
50. Wang H et al. Dual-color ultrasensitive bright-field RNA in situ hybridization with RNAscope. Methods Mol. Biol 1211, 139–149 (2014). [PubMed: 25218383]
51. Murphey RD, Stern HM, Straub CT & Zon LIA chemical genetic screen for cell cycle inhibitors in zebrafish embryos. Chem. Biol. DrugDes 68, 213–219 (2006).

Author Manuscript Author Manuscript Author Manuscript Author Manuscript

52. Mazzocco C et al. In vivo imaging of prostate cancer using an anti-PSMA scFv fragment as a probe. Sci. Rep 6, 23314 (2016). [PubMed: 26996325]

53. Curado S et al. Conditional targeted cell ablation in zebrafish: a new tool for regeneration studies. Dev. Dyn 236, 1025–1035 (2007). [PubMed: 17326133]

54. Chudakov DM, Lukyanov S & Lukyanov KA Using photoactivatable fluorescent protein Dendra2 to track protein movement. Biotechniques 42, 10.2144/000112470 (2007).

55. Chudakov DM, Lukyanov S & Lukyanov KA Tracking intracellular protein movements using photoswitchable fluorescent proteins PS-CFP2 and Dendra2. Nat. Protocols 2, 2024–2032 (2007). [PubMed: 17703215]

56. Chen Q et al. Haemodynamics-driven developmental pruning of brain vasculature in zebrafish. PLoS Biol. 10, e1001374 (2012). [PubMed: 22904685]

57. Kamoun WS et al. Simultaneous measurement of RBC velocity, flux, hematocrit and shear rate in vascular networks. Nat. Methods 7, 655–660 (2010). [PubMed: 20581828]

58. Schaffer CB et al. Two-photon imaging of cortical surface microvessels reveals a robust redistribution in blood flow after vascular occlusion. PLoS Biol. 4, e22 (2006). [PubMed: 16379497]

Author Manuscript Author Manuscript Author Manuscript Author Manuscript

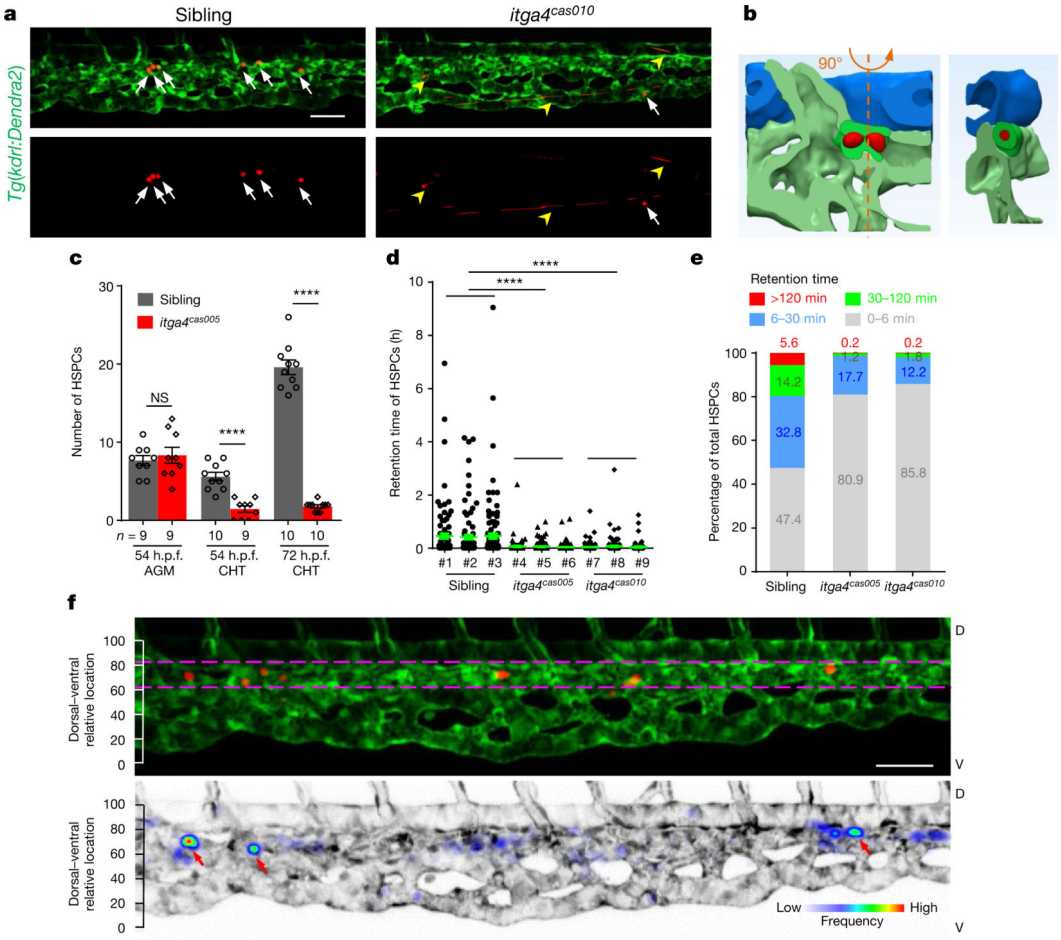

Fig. 1 |. Live-imaging characterization of nascent HSPCs retention in the cHt.

a, Frame shots from the CHT at 54 h.p.f. show HSPCs seeding successfully (white arrows) in wild-type siblings but not in *itga4*^{cas010} mutants (fast moving, yellow arrowheads). See Supplementary Video 1. **b,** A representative vascular architecture view of the HSPC retention hotspot. The orthogonal view is shown on the right. HSPCs, red; dorsal aorta, blue; venous plexus, light green; venous capillary, dark green. See Supplementary Video 4. **c,** The number of HSPCs in the AGM and CHT ol *itga4*^{cas005} mutants and wild-type siblings at 54 and 72 h.p.f., respectively. 54 h.p.f. AGM: $P = 0.59$, $t = 0.55$, df = 16; 54 h.p.f. CHT: ****$P < 0.0001$, $t = 6.00$, df = 17; 72 h.p.f. CHT: ****$P < 0.0001$, $t = 18.65$, df = 18. NS, not significant. **d, e,** Retention time of individual HSPCs in each embryo (**d**) and percentage of total HSPCs in four classified retention time zones in group embryos ($n = 3$) (**e**) of wild-type siblings and *itga4*^{cas005} and *itga4*^{cas005} mutants during 50–60 h.p.f. Wild type vs *itga4*^{cas005}: $P < 0.0001$, $t = 8.56$, df = 824; wild type vs *itga4*^{cas010}: $P < 0.0001$, $t = 7.93$, df = 758. **f,** Top, HSPCs that remained for longer than 30 min were preferentially located in the region enriched with venous capillaries (between the two magenta dashed lines). Bottom, the frequency of the appearance of HSPCs in the entire CHT of *Tg(kdrl:Dendra2)* zebrafish larvae from 50 to 60 h.p.f. (retention hotspots marked by red arrows). D, dorsal; V, ventral. Scale bars, 50 μm (**a, f**).

Author Manuscript Author Manuscript Author Manuscript Author Manuscript

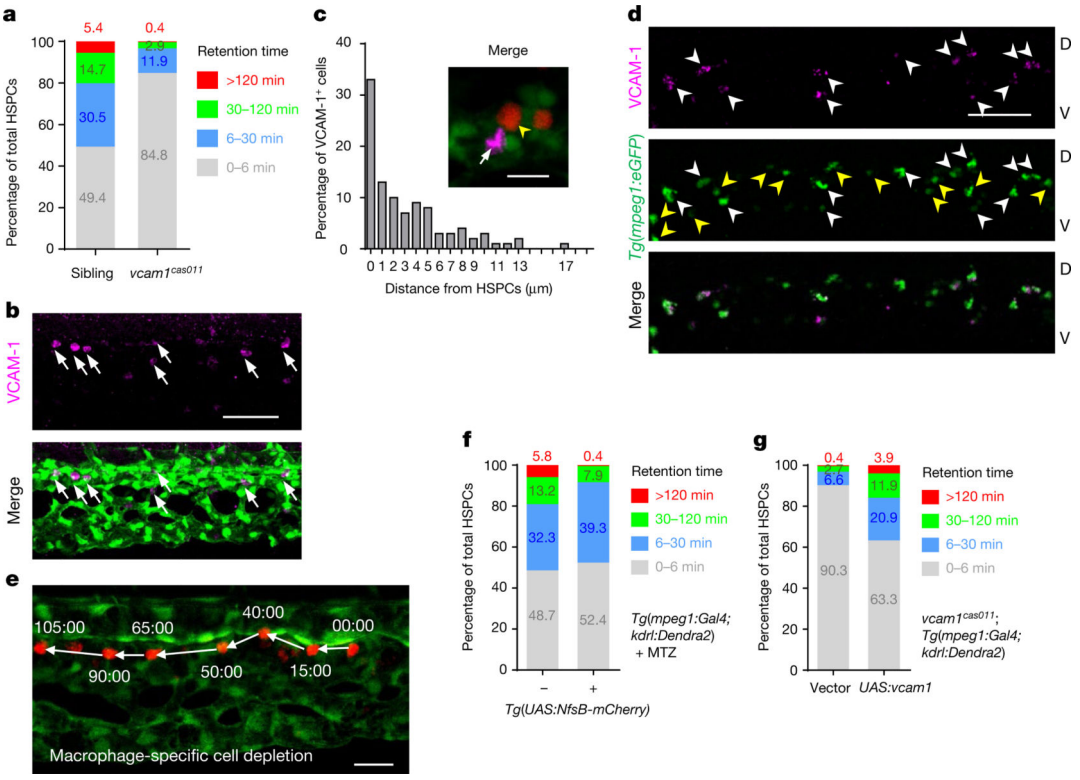

Fig. 2 |. Distinct role of macrophages and venous endothelium VCAM-1 in HSPCs retention.

a, Percentage of total HSPCs in four classified retention time zones in grouped wild-type siblings and *vcam1*^{cas011} mutants (n = 3) at 50–60 h.p.f. **b,** *Tg*(*kdrl:eGFP*) embryos, stained with an anti-VCAM-1 antibody (magenta, arrows), show dorsal venous plexus distribution of individual VCAM-1^{+} cells in the CHT. **c,** Percentage of VCAM-1^{+} cells in the CHT scored by the distance to the nearest HSPC (edge to edge, *n* = 100). Most (86%; 86 out of 100 cells) VCAM-1^{+} cells were located within 7 μm of HSPCs (the average diameter of HSPCs is about 6.9 μm). *Tg(kdrl:Dendra2)* embryos with AGM photoconversion were stained with an anti-VCAM-1 antibody (magenta, white arrow). Yellow arrowheads denote HSPCs. **d,** The staining of *Tg(mpeg1:eGFP)* embryos with an anti-VCAM-1 antibody (magenta) shows that VCAM-1^{+} cells merge with *mpeg1*$^{+}$ cells (green) in the CHT. White arrowheads denote VCAM-1^{+}GFP^{+} double-positive cells; yellow arrowheads denote GFP single-positive cells. **e,** Live-imaging frame shots of HSPCs in macrophage-specific cell-depletion embryos from **f**. See Supplementary Video 6. Time is in minutes:seconds. **f,** Percentage of total HSPCs in four classified retention time zones in grouped (*n* = 3) *Tg(mpeg1:Gal4,kdrl:Dendra2)* embryos with MTZ treatment, with or without the *Tg(UAS:NfsB-mCherry)* background, at 50–60 h.p.f. **g,** Percentage of total HSPCs in four classified retention time zones in grouped (n = 3) *vcam1*^{cas011} mutants in a *Tg(mpeg1:Gal4,kdrl:Dendra2)* background with transient transgenesis of either vector (UAS*:polyA)* or *UAS:vcam1* at 50–60 h.p.f. See Supplementary Video 6. Scale bars, 50 μm (**b, d**), 20 μm (**e**) and 10 μm (**c**).

Author Manuscript Author Manuscript Author Manuscript Author Manuscript

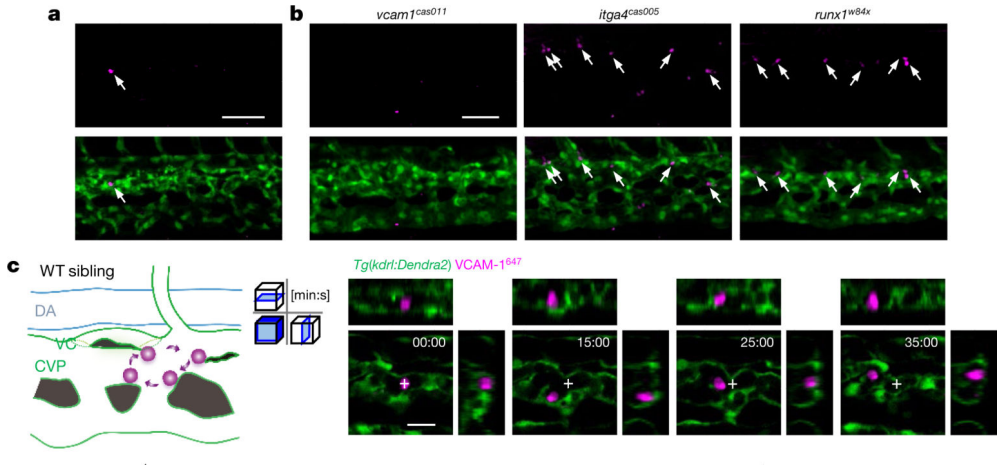

Fig. 3 |. Characterization of VCAM-1^{+} macrophages in the CHT.

a, Transgenic *Tg(kdrl:eGFP)* embryos, stained with an anti-VCAM-1 antibody (magenta, arrows), show that the VCAM-1^{+} macrophage first appeared in the CHT at 32 h.p.f. **b,** *Tg(kdrl:eGFP)* embryos in the *vcam1*^{cas011}, *itga4*^{cas005} or *runx1*^{w84x} mutant background are stained with an anti-VCAM-1 antibody (magenta, white arrows) at 54 h.p.f. Signals in *itga4*^{cas005} and *runx1*^{w84x} are similar to that in wild-type siblings, whereas there is almost no detectable signal in *vcam1*^{cas011} mutants. **c,** Schematic diagrams (left) and confocal imaging (right) of VCAM-1^{+} macrophages (labelled with Alexa Fluor 647 dye-conjugated anti-VCAM-1 antibody by intravascular injection) that patrol the CHT of wild-type embryos. VCAM-1^{+} macrophages were mainly located intravascularly (>91%) with round or unpolarized cell morphology (>84%). Cross indicates the original position of VCAM-1^{+} macrophages at the initial imaging time point. See Supplementary Video 7. DA, dorsal aorta; VC, venous capillaries. Scale bars, 50 μm (**a, b**) and 20 μm (**c**).

Author Manuscript Author Manuscript Author Manuscript Author Manuscript

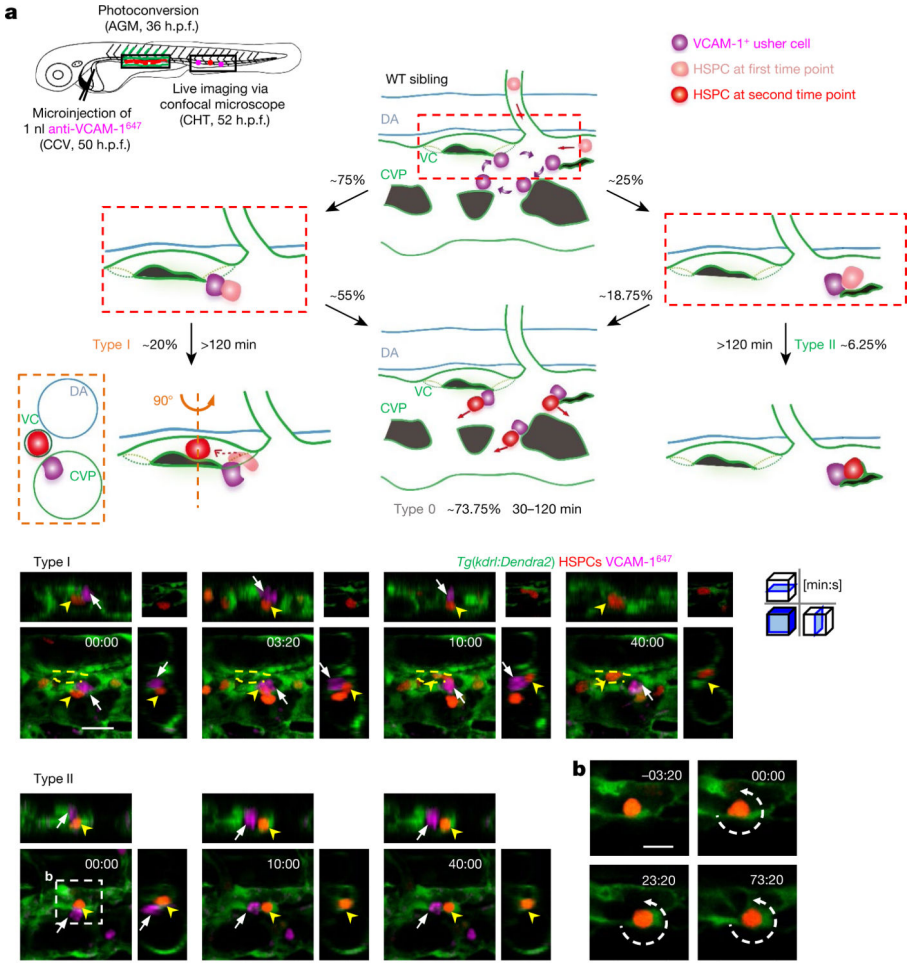

Fig. 4 |. Live imaging analysis on VCAM-1^{+} usher cell-guided HSPCs retention.

a, Schematic illustration (top left) shows that labelling of HSPCs (with photoconverted Dendra2, red) was performed at 36 h.p.f. in *Tg(kdrl:Dendra2)* embryos, followed by an anti-VCAM-1^{647} antibody injection at 50 h.p.f. Live imaging was performed 2 h after injection (52 h.p.f.). Schematic diagrams (top) show the HSPC retention model, with accurate percentage and classification. See Supplementary Table 3. Representative images (bottom) show the interaction between HSPCs (red; yellow arrowheads) and VCAM-1^{+} usher cells (magenta; white arrows). VCAM-1^{+} usher cells guide HSPCs into the venous capillaries, leading to type I and II retention (see Supplementary Videos 8 and 9). The top right images show one slice, and the others show *z*-stacks. **b,** Enlarged view of endothelial cell remodelling around a single HSPC to form a stem-cell pocket in type II retention (see Supplementary Video 9). Scale bars, 20 μm (**a**) and 10 μm (**b**).